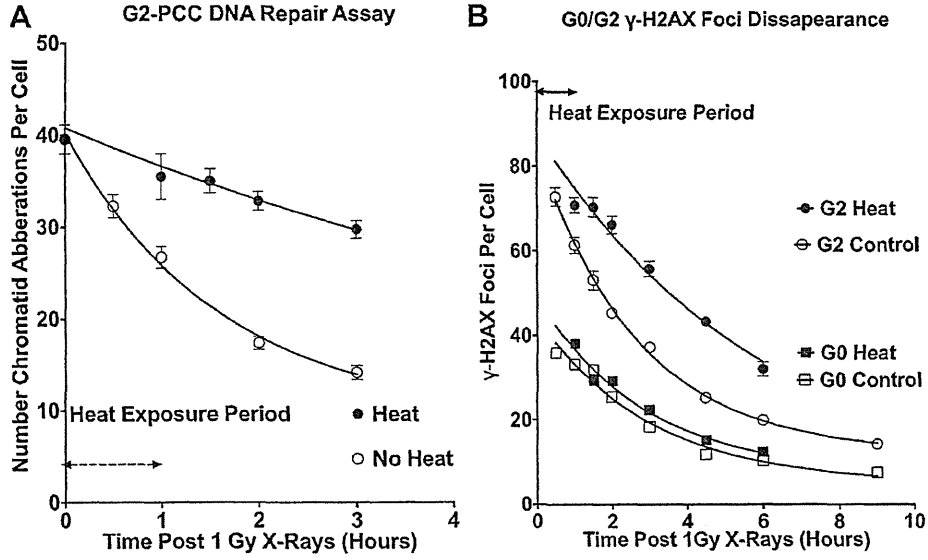

Fig. 3. A: Evaluating DNA-repair capabilities of AG1521 cells via premature chromatin condensation: AG1521 cells were exposed to either 1 Gy of X-rays or 1 Gy of X-rays followed by a 1 h 42.5°C hyperthermic treatment, and G2 chromosomes subjected to PCC were analyzed. Cells exposed to hyperthermia–radiation conjunctive treatments are depicted as closed circles, and radiation-alone treatments are depicted as open circles. All experiments were carried out at least three times and error bars depict the standard error of the means. B: Evaluating DNA-repair capabilities of AG1521 cells via γ-H2AX Immunocytochemistry: AG1521 cells were exposed to either 1 Gy of X-rays or 1 Gy of X-rays followed by a 1 h 42.5°C hyperthermic treatment, and G2 (open/closed circles) or G0 (open/closed squares) phase cells were analyzed. Error bars indicate standard error of the means from three independent experiments.

was used for experiments depicted in Fig. 4C, Rad51 foci returned and co-localizations with γ-H2AX foci were again observed at 6–8 h for 42.5°C heating and 8–10 h for 44.5°C hyperthermia (Figs. 4C and 5.) These data show Rad51/γ-H2AX co-localization recovery time as being related to hyperthermic exposure in a time- and temperature-dependent manner.

Discussion

Collectively, our studies have shown that hyperthermia inhibits homologous recombination DNA repair in a time- and temperature-dependent manner (Figs. 2A,B, 3A,B, 4A–C, and 5). Subsequently, the temperature and time of hyperthermia application to a tumor during the course of radiation therapy will proportionately reduce malignant cell's ability to repair radiation-induced DNA double strand breaks via the homologous recombination pathway. Rad51 was identified as the major DNA repair protein target of hyperthermia, and the inhibition of this protein's DNA repair abilities translates to cells' reduced ability to survive following a radiotoxic insult. Our results reflect previous studies observation that hyperthermia inhibits homologous recombination repair following exposure to ionizing radiation (Krawczyk et al., 2011). Knock out and gene complimented versions of various DNA repair proteins were used in our study to display the major DNA repair pathway target of hyperthermia in radiation therapy. Observed wild-type and non-homologous end joining mutant V3 hyperthermia-induced radio-sensitivity, and the lack of this effect in cell lines deficient in homologous recombination repair suggests the homologous recombination repair mechanism is inhibited by hyperthermic conditions during hyperthermia-radiation conjunctive treatments (Fig. 2A). Fanconi Anemia mutant KO40 also displayed this hyperthermia-induced radio-sensitization effect. This is an interesting finding considering the FancG protein has been shown to be involved with homologous recombination (Yamamoto et al., 2003). This result may suggest potential differences between homologous recombination repair and fanconi pathway. G2 cell populations proficient in homologous recombination repair (i.e., wild-type cells and non-homologous end joining mutants) displayed marked hyperthermia-induced radio-sensitization relative to synchronized G0 populations, which provides additional evidence for homologous recombination being a major target of hyperthermia during conjunctive treatments with radiation (Fig. 2B). Moreover, additional support for hyperthermia acting as an inhibitor of homologous recombination was observed in AG1521 cells selected in G2 phase following hyperthermia-radiation conjunctive treatments, which most notably displayed a decreased ability to diminish both DNA double strand breaks and subsequent chromatid aberrations post-treatment (Fig. 3A,B).

As stated above, we were able to show a major homologous recombination protein, Rad 51, dissociate from DNA double strand breaks in response to hyperthermia following exposure to gamma rays in order to provide conformational evidence of defective homologous recombination during hyperthermia-induced radio-sensitization. Rad51 dissociation from DNA double strand breaks in response to varying hyperthermic conditions reflected this time–temperature-dependent trend accompanying cell survival data in response to heat alone, which suggests the loss of function of this particular protein in response to hyperthermia treatments following exposure to ionizing radiation plays a significant role in hyperthermia-induced radio-sensitization. Changes in cell killing time trends in response to heat alone (derived most notably via 10% cell survival values from inverse-isoeffect plots) was identifiable at and above 42.5°C for wild-type cells in response to heat alone. Interestingly, we were able to see Rad51 dissociate from DNA double strand break foci using wild-type cells in a trend (relative to un-heated 37°C control irradiated samples) that mirrored

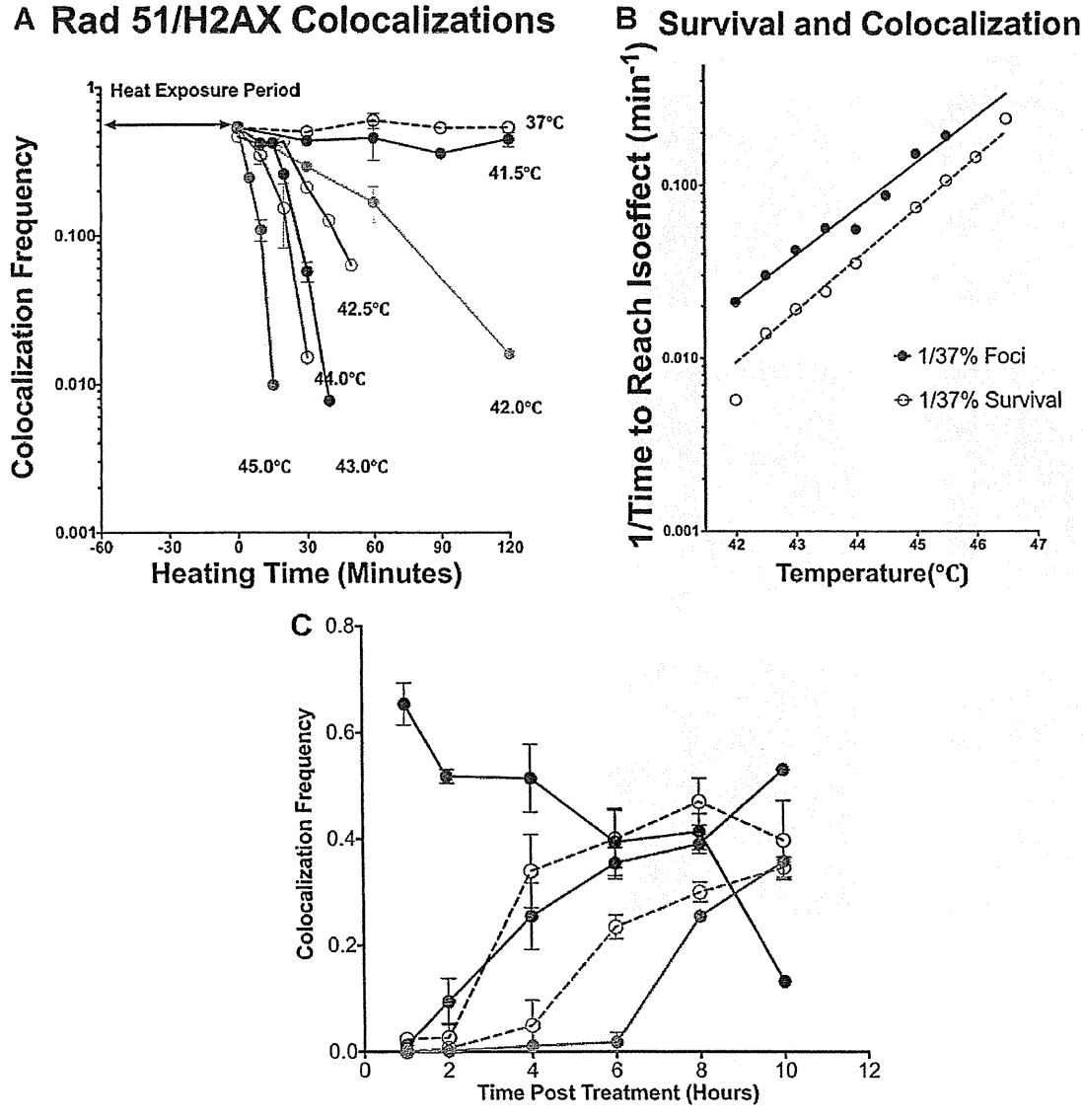

Fig. 4. **A: Evaluation of Rad-51 repair of DNA double strand breaks in response to hyperthermia–radiation conjunctive treatments: Exponentially proliferating wild-type cells were exposed to time/temperature varying hyperthermic conditions following exposure to 1 Gy of gamma rays and a 1-h post-irradiation incubation period. The number of cells with Rad51/γ-H2AX co-localizations out of a population of >100 cells was scored in a time-progressive manner to evaluate homologous recombination repair efficiency. Error bars indicate standard error of the means of at least three independent experiments. B: Inverse Isoeffect plot of Rad51/γ-H2AX co-localization data: Rad51/γ-H2AX co-localization data were analyzed via an inverse isoeffect plot displaying a significant reduction of Rad51 DNA repair activity around 43°C. "1/time to reach isoeffect" values were represented as the inverse time of hyperthermia exposure required to reduce a population of cells' Rad51/γ-H2AX co-localization frequencies to a discrete percentage (50, 37, or 10%) of wild-type CHO cells exposed to 1 Gy of gamma rays alone with no hyperthermic conditions (i.e., 37°C) following irradiation. C: Restoration of Rad51 associations with DNA double strand breaks over time: Exponentially proliferating wild-type cells were immediately exposed to varying hyperthermic conditions following exposure to 1 Gy of gamma rays in order to analyze Rad51/γ-H2AX co-localization frequency. Cells heated at 42.5°C for either 40 or 60 min (open and closed circles, respectively), and 44.5°C for either 20 or 40 min (open and closed circles, respectively), and 37°C control for closed black circles. Error bars indicate standard error of the means of at least four experiments.**

the cell survival data trend below, at, and above this 42.5°C threshold temperature. These findings suggest the level of homologous recombination inhibition resulting from Rad51 dissociation from DNA double strand break sites is positively correlated to the time and temperature of hyperthermia exposure. These findings, although interesting, may have limited applicability regarding temperatures exceeding 42.0°C at the in vivo level due to blood flow carrying heat away from a tumor where hyperthermia treatments are localized (Song et al., 2005). Using a xenobiotic to decrease blood flow to a tumor could potentially allow tumors to be heated to higher temperatures at the clinical level, however, employing this approach may actually decrease tumor control due to an increased prevalence of hypoxic conditions in malignant cells, which is well known to contribute to radioresistance. Nevertheless, protocols dictating time and temperature application of hyperthermia in radiotherapy can be manipulated (when feasible) to maximize tumor control.

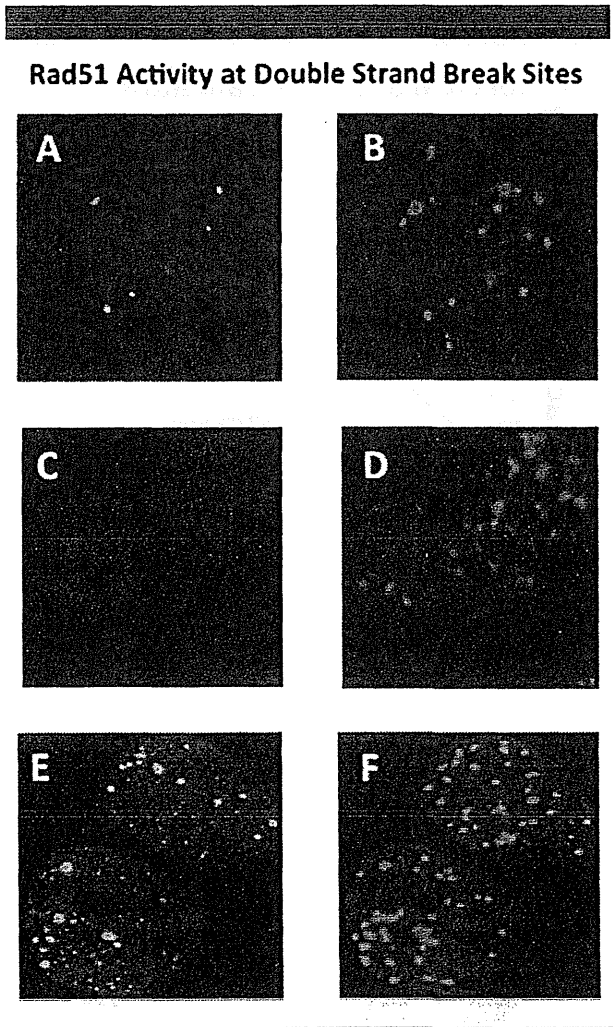

Fig. 5. Examples of scoring populations of wild-type cells using immunocytochemisty for Rad 51/γ-H2AX co-localizations: γ-H2AX foci are shown in right columns as red and Rad51 foci are shown in left columns as green. DAPI is shown in blue. Images A and B represent cells 4-h post-treatment (of 1 Gy of X-rays and a 1-h incubation period) cells held at 37°C following gamma-ray exposure are indicative of Rad51 functioning, whereas images C and D taken 2-h post-treatment of cells held at 44.5°C following gamma-ray exposure and 1-h incubation period are indicative of Rad51 loss of activity. Images E and F represent Rad51 recovery at a time point of 10-h post 1 Gy gamma-ray exposure.

Our results displaying Rad51's re-association with DNA double stand break foci shows that this protein's dissociation in response to hyperthermia is only a temporary phenomena, and the time required for this protein to reform with DNA double strand break sites following hyperthermia treatments post-irradiation is dependent again on time and temperature of exposure to hyperthermia. These results reflect previous reporting of hyperthermia-induced radio-sensitization's effects being only temporary, therefore, time-restricted regarding radio therapeutic effectiveness (Sapareto et al., 1978). The time and level of which Rad51 proteins re-associate with DNA double strand break sites was positively correlated with time and temperature of hyperthermia application, and this highlights the potential to optimize tumor control in radiation therapy by manipulating hyperthermia application.

The presence of Rad51, and potentially other homologous recombination proteins, in malignant cells is a key tenet for effective hyperthermia-induced radio sensitization. From a clinical perspective, this phenomenon can be utilized to optimize treatment by means of maximizing tumor control in tumors possessing cells with Rad51 (and potentially other homologous recombination proteins displaying similar responses to hyperthermia and radiation conjunctive treatments as those of Rad51 in this study) positive genotypes. An admonition to prudent radiation oncologists may be to opt out of hyperthermia treatments in addition to radiation therapy for patient's whose malignancies display Rad51 (and potentially other homologous recombination proteins) negative genotypes in order to spare unwanted effects to rapidly proliferating healthy tissues whose cells are homologous recombination proficient. Homologous recombination requires a complex interplay of several proteins that all potentially serve as targets for hyperthermia treatments in conjunction with DNA double strand break causative agents. A recent study identified several of these other homologous recombination proteins, MRE11, BRCA2, and RPA34 as targets for hyperthermia in addition to Rad51, which reinforces our findings (Krawczyk et al., 2011). However, whether or not these other homologous recombination proteins dissociate from DNA double strand break sites and subsequently reform to these same sites in a manner similar to, or differing from, our reported results remains unknown and an interesting topic for further research. Pending further elucidation of hyperthermia's interplay with these various homologous recombination proteins, more effective hyperthermia–radiation conjunctive treatment protocols may be realized and implemented for therapies for certain types of cancers where hyperthermia will maximize tumor control (i.e., malignancies that possess positive homologous recombination genotypes) without causing excessive repercussive effects to healthy tissues.

Acknowledgments

This study is partially supported by start-up fund from Colorado State University (T.A. Kato) and College Research Council fund (T.A. Kato) from the College of Veterinary Medicine and Biomedical Sciences, Colorado State University.

Literature Cited

Bhuyan BK. 1979. Kinetics of cell kill by hyperthermia. Cancer Res 39:2277–2284.
Deorukhakar VV, Anjaria KB, Rao BS. 1993. Modification of radiation-induced damage by hyperthermia—Role of repair processes. Int J Hyperthermia 9:803–810.
Dewey WC, Hopwood LE, Sapareto SA, Gerweck LE. 1977. Cellular responses to combinations of hyperthermia and radiation. Radiology 123:463–474.
Dynlacht JR, Bittner ME, Bethel JA, Beck BD. 2003. The non-homologous end-joining pathway is not involved in the radiosensitization of mammalian cells by heat shock. J Cell Physiol 196:557–564.
Dynlacht JR, Xu M, Pandita RK, Wetzel EA, Roti Roti JL. 2004. Effects of heat shock on the Mre11/Rad50/Nbs1 complex in irradiated or unirradiated cells. Int J Hyperthermia 20:144–156.
Hahn GM. 1974. Metabolic aspects of the role of hyperthermia im mammalian cell inactivation and their possible relevance to cancer treatment. Cancer Res 34:3117–3123.
Hinz JM, Tebbs RS, Wilson PF, Nham PB, Salazar EP, Nagasawa H, Urbin SS, Bedford JS, Thompson LH. 2006. Repression of mutagenesis by Rad51D-mediated homologous recombination. Nucleic Acids Res 34:1358–1368.
Iliakis G, Seaner R. 1990. A DNA double-strand break repair-deficient mutant of CHO cells shows reduced radiosensitization after exposure to hyperthermic temperatures in the plateau phase of growth. Int J Hyperthermia 6:801–812.
Iliakis G, Wu W, Wang M. 2008. DNA double strand break repair inhibition as a cause of heat radiosensitization: Re-evaluation considering backup pathways of NHEJ. Int J Hyperthermia 24:17–29.
Kampinga HH, Dynlacht JR, Dikomey E. 2004. Mechanism of radiosensitization by hyperthermia (> or =43°C) as derived from studies with DNA repair defective mutant cell lines. Int J Hyperthermia 20:131–139.
Kato TA, Okayasu R, Bedford JS. 2008. Comparison of the induction and disappearance of DNA double strand breaks and gamma-H2AX foci after irradiation of chromosomes in G1-phase or in condensed metaphase cells. Mutat Res 639:108–112.
Krawczyk PM, Eppink B, Essers J, Stap J, Rodermond H, Odijk H, Zelensky A, van Bree C, Stalpers LJ, Buist MR, Soullie T, Rens J, Verhagen HJ, O'Connor MJ, Franken NA, Ten Hagen TL, Kanaar R, Aten JA. 2011. Mild hyperthermia inhibits homologous recombination, induces BRCA2 degradation, and sensitizes cancer cells to poly (ADP-ribose) polymerase-1 inhibition. Proc Natl Acad Sci USA 108:9851–9856.
Laszlo A, Fleischer I. 2009. Heat-induced perturbations of DNA damage signaling pathways are modulated by molecular chaperones. Cancer Res 69:2042–2049.

Mitchel RE, Birnboims HC. 1985. Triggering of DNA strand breaks by 45 degrees C hyperthermia and its influence on the repair of gamma-radiation damage in human white blood cells. Cancer Res 45:2040–2045.
Nevaldine B, Longo JA, Hahn PJ. 1994. Hyperthermia inhibits the repair of DNA double-strand breaks induced by ionizing radiation as determined by pulsed-field gel electrophoresis. Int J Hyperthermia 10:381–388.
Raaphorst GP, Thakar M, Ng CE. 1993. Thermal radiosensitization in two pairs of CHO wild-type and radiation-sensitive mutant cell lines. Int J Hyperthermia 9:383–391.
Raaphorst GP, Yang DP, Niedbala G. 2004. Is DNA polymerase beta important in thermal radiosensitization? Int J Hyperthermia 20:140–143.
Rice GC, Gray JW, Dean PN, Dewey WC. 1984. Fluorescence-activated cell sorting analysis of the induction and expression of acute thermal tolerance within the cell cycle. Cancer Res 44:2368–2376.
Roti Roti JL. 2007. Heat-induced alterations of nuclear protein associations and their effects on DNA repair and replication. Int J Hyperthermia 23:3–15.
San Filippo J, Sung P, Klein H. 2008. Mechanism of eukaryotic homologous recombination. Annu Rev Biochem 77:229–257.
Sapareto SA, Hopwood LE, Dewey WC. 1978. Combined effects of X irradiation and hyperthermia on CHO cells for various temperatures and orders of application. Radiat Res 73:221–233.
Song CW, Park HJ, Lee CK, Griffin R. 2005. Implications of increased tumor blood flow and oxygenation caused by mild temperature hyperthermia in tumor treatment. Int J Hyperthermia 21:761–767.
Takahashi A, Matsumoto H, Nagayama K, Kitano M, Hirose S, Tanaka H, Mori E, Yamakawa N, Yasumoto J, Yuki K, Ohnishi K, Ohnishi T. 2004. Evidence for the involvement of double-strand breaks in heat-induced cell killing. Cancer Res 64:8839–8845.
Tebbs RS, Hinz JM, Yamada NA, Wilson JB, Salazar EP, Thomas CB, Jones IM, Jones NJ, Thompson LH. 2005. New insights into the Fanconi anemia pathway from an isogenic FancG hamster CHO mutant. DNA Repair (Amst) 4:11–22.
Tobey RA, Ley KD. 1970. Regulation of initiation of DNA synthesis in Chinese hamster cells. I. Production of stable, reversible G1-arrested populations in suspension culture. J Cell Biol 46:151–157.
van der Zee J, Vujaskovic Z, Kondo M, Sugahara T. 2008. The Kadota Fund International Forum 2004—Clinical group consensus. Int J Hyperthermia 24:111–122.
Westra A, Dewey WC. 1971. Variation in sensitivity to heat shock during the cell-cycle of Chinese hamster cells in vitro. Int J Radiat Biol Relat Stud Phys Chem Med 19:467–477.
Weterings E, Chen DJ. 2008. The endless tale of non-homologous end-joining. Cell Res 18:114–124.
Xu M, Myerson RJ, Xia Y, Whitehead T, Moros EG, Straube WL, Roti JL. 2007. The effects of 41 degrees C hyperthermia on the DNA repair protein, MRE11, correlate with radiosensitization in four human tumor cell lines. Int J Hyperthermia 23:343–351.
Yamamoto K, Ishiai M, Matsushita N, Arakawa H, Lamerdin JE, Buerstedde JM, Tanimoto M, Harada M, Thompson LH, Takata M. 2003. Fanconi anemia FANCG protein in mitigating radiation- and enzyme-induced DNA double-strand breaks by homologous recombination in vertebrate cells. Mol Cell Biol 23:5421–5430.

EMBO reports

EMBO open

scientific report

Synaptonemal complex protein SYCP3 impairs mitotic recombination by interfering with BRCA2

Noriko Hosoya[1+], Miyuki Okajima[1], Aiko Kinomura[2,3], Yoshihiro Fujii[1], Takashi Hiyama[2,4], Jiying Sun[3], Satoshi Tashiro[3] & Kiyoshi Miyagawa[1++]

[1]Laboratory of Molecular Radiology, Center for Disease Biology and Integrative Medicine, Graduate School of Medicine, University of Tokyo, Tokyo, [2]Department of Human Genetics, [3]Department of Cellular Biology, Research Institute for Radiation Biology and Medicine, and [4]Department of Surgery, Graduate School of Biomedical Sciences, Hiroshima University, Hiroshima, Japan

The meiosis-specific synaptonemal complex protein SYCP3 has been reported to be aberrantly expressed in tumours. However, in contrast to its well-defined function in meiosis, its possible role in mitotic cells is entirely unknown. Here, we show that SYCP3 is expressed in a range of primary tumours and that it impairs chromosomal integrity in mitotic cells. Expression of SYCP3 inhibits the homologous recombination (HR) pathway mediated by RAD51, inducing hypersensitivity to DNA-damaging agents such as a poly(ADP-ribose) polymerase (PARP) inhibitor and chromosomal instability. SYCP3 forms a complex with BRCA2 and inhibits its role in HR. These findings highlight a new mechanism for chromosomal instability in cancer and extend the range of PARP-inhibitor sensitive tumours to those expressing SYCP3.

Keywords: chromosomal instability; homologous recombination; meiosis-specific protein

EMBO *reports* (2012) 13, 44–51. doi:10.1038/embor.2011.221

INTRODUCTION

SYCP3 is a component of the synaptonemal complex, a meiosis-specific supramolecular proteinaceous structure essential for synapsis of the maternal and paternal homologous chromosomes (Page & Hawley, 2004). Although SYCP3 was first considered to be a meiosis-specific protein, it has been reported to be aberrantly expressed in human leukaemia and primary cervical cancers (Niemeyer *et al*, 2003; Kang *et al*, 2010), suggesting that SYCP3 is a member of cancer/testis antigens whose expression is normally limited to the germ cells but abnormally activated in cancer (Simpson *et al*, 2005). However, although the meiotic role of SYCP3 is well characterized, its mitotic role is entirely unknown.

Homologous recombination (HR) is one of the main pathways in the repair of DNA double-strand breaks (DSBs) in mitotic cells (Hartlerode & Scully, 2009). RAD51 has a central role in the early stages of HR. The breast cancer susceptibility protein BRCA2 binds to RAD51 and recruits it to the sites of DSBs and promotes RAD51 filament formation, which is essential for the subsequent homologous DNA pairing and strand-exchange steps of HR (Gudmundsdottir & Ashworth, 2006).

In this study, we investigated the role for SYCP3 in mitotic cells. We show that SYCP3 inhibits the mediator role of BRCA2 in HR and induces chromosomal instability by impairing the intrinsic repair pathway. As SYCP3 is expressed in various tumour types, our finding suggests that inactivation of HR by SYCP3 might be prevalent in cancer.

RESULTS

SYCP3 is expressed in various tumours

We first examined the expression profiles of SYCP3 in two non-cancerous normal human cells and 16 human cancer cell lines by western blot analysis. Although no expression of SYCP3 was detected in the normal retinal pigmented epithelial cell line RPE and the normal human mammary epithelial cell line HME, SYCP3 was aberrantly expressed in various cancer cell lines (supplementary Fig S1A online). The hepatocellular carcinoma cell line HepG2 and the prostate cancer cell line DU145 showed moderate expression levels, whereas most of other cancer cells showed low expression levels compared with the high expression levels observed in normal testis. Although *SYCP3* expression was not detected in the colorectal carcinoma cell line DLD1, its expression was induced in DLD1 cells after treatment with the demethylating agent 5-azacytidine (supplementary Fig S1B online), indicating that *SYCP3* expression in mitotic cells is regulated by a demethylation-dependent process, which is in agreement with the previous report (Maatouk *et al*, 2006).

[1]Laboratory of Molecular Radiology, Center for Disease Biology and Integrative Medicine, Graduate School of Medicine, University of Tokyo, Tokyo 113-0033
[2]Department of Human Genetics,
[3]Department of Cellular Biology, Research Institute for Radiation Biology and Medicine, and
[4]Department of Surgery, Graduate School of Biomedical Sciences, Hiroshima University, Hiroshima 734-8553, Japan
[+]Corresponding author. Tel: +81 3 5841 3505; Fax: +81 3 5841 3013;
E-mail: nhosoya-tky@umin.ac.jp
[++]Corresponding author. Tel: +81 3 5841 3505; Fax: +81 3 5841 3013;
E-mail: miyag-tky@umin.ac.jp

Received 18 February 2011; revised 11 September 2011; accepted 18 October 2011; published online 25 November 2011

To evaluate the expression pattern of *SYCP3* in human primary tumours, we analysed its expression by using an mRNA array that contained two duplicated spots of mRNA from 47 different tumours and 47 normal tissues from unmatched donors (supplementary Fig S2A and Table S1 online). The array was probed for expression of *SYCP3* and *β-actin*, and the signal ratios of *SYCP3/β-actin* from the two duplicated spots were averaged. Whereas almost all the normal samples showed low levels of signal ratios, significantly increased levels of *SYCP3/β-actin* signal ratios were observed in one adrenal tumour, three liver tumours, one stomach tumour and one kidney tumour (supplementary Fig S2B online). Although one normal liver sample showed a high level of the signal ratio, its biological significance is unknown because the profile of the donor is not available. These findings indicate that *SYCP3* expression is not specific to certain tumour types but is observed in tumours of various tissue origins.

DNA damage is accumulated by expression of SYCP3

To investigate the role of SYCP3 expression in mitotic cells, we established two independent RPE clones stably expressing SYCP3 at low levels comparable with endogenous levels in cancer such as the fibrosarcoma cell line HT1080 (supplementary Fig S3A online). Immunofluorescence detection of nuclear foci of γH2AX, the phosphorylated form of histone H2AX, which is recruited to DSBs in response to DNA damage, revealed an increase in the frequency of foci-positive cells after forced SYCP3 expression from 5.5 ± 1.5% (mean ± s.d.) in mock cells to 17.5 ± 0.5% and 19.5 ± 0.5% in the two SYCP3-expressing RPE clones, respectively (Fig 1A,B). These results indicate an accumulation of DSBs in SYCP3-expressing cells.

Expression of SYCP3 leads to increased aneuploidy

We next examined the frequency of aneuploidy by fluorescence *in situ* hybridization analysis using two independent chromosome-specific centromeric probes (Fig 1C,D). Results showed a significant increase in aneuploidy frequency at chromosome 7 from 4.3 ± 0.3% in mock cells to 9.8 ± 1.2% and 12.1 ± 0.5% in SYCP3-expressing RPE cells ($P<0.05$, Fisher's exact test). At chromosome 17, the frequency also increased from 3.5 ± 0.6% to 8.8 ± 1.5% and 12.6 ± 0.6% ($P<0.05$). These results indicate that expression of SYCP3 leads to increased aneuploidy in mitotic cells.

SYCP3 confers hypersensitivity to DNA damage

Next, we examined the sensitivity of SYCP3-expressing RPE cells to DNA damage by measuring their ability to form colonies after exposure to ionizing radiation (IR) or cisplatin, an interstrand crosslinking agent. Results showed a roughly twofold increase in sensitivity to IR and cisplatin after expression of SYCP3 (Fig 1E,F). These findings indicate that expression of SYCP3 regulates sensitivity to DNA damage, which includes DSBs.

SYCP3 decreases IR-induced RAD51 foci formation

DSBs are repaired by either HR or non-homologous end-joining. As deficiency in HR but not in non-homologous end-joining leads to hypersensitivity to DNA crosslinking agents (Nojima *et al*, 2005), we assumed that expression of SYCP3 inhibits the HR pathway. RAD51 forms nuclear foci in S and G2 phases in a DNA damage-dependent manner (Tashiro *et al*, 2000). We therefore assessed the IR-induced foci formation of several recombination molecules including RAD51 in RPE clones stably expressing FLAG–SYCP3 at levels comparable with that of endogenous expression in HepG2 cells (supplementary Fig 3B online).

A decrease in the frequency of IR-induced RAD51 foci-positive cells was observed after stable SYCP3 expression from 66.3 ± 0.6% (mean ± s.d.) in mock cells to 37.3 ± 6.3% and 44.0 ± 4.0% in the two FLAG–SYCP3-expressing RPE clones (Fig 2A,B). The protein levels of RAD51 were similar in mock and FLAG–SYCP3-expressing cells (supplementary Fig S4A online), suggesting that expression of SYCP3 inhibits the recruitment but not the expression levels of RAD51 after DNA damage. The cell populations in S phase were almost similar between mock and FLAG–SYCP3-expressing cells (supplementary Fig 4B online), suggesting that impaired IR-induced RAD51 foci formation was not due to a decrease in the number of cells in S phase. The frequency of IR-induced RAD51 foci-positive cells in cells in S and G2 phases was also examined by double staining of RAD51 with cyclin A (Fig 2C), and a robust decrease from 96.7 ± 0.6% in mock cells to 59.0 ± 3.6% and 67.3 ± 6.8% in the two FLAG–SYCP3-expressing RPE clones was observed (Fig 2D).

No differences were observed in the foci formation of NBS1, which functions upstream of RAD51 in a complex with MRE11 and RAD50 in response to DNA damage, or in foci formation of BRCA1, which is indirectly associated with RAD51 (supplementary Fig S4C–F online). These observations indicate that SYCP3 affects the molecules in close proximity to RAD51.

Knockdown of SYCP3 recovers the function of RAD51

Next, we evaluated the IR-induced foci formation of recombination molecules by reducing SYCP3 expression in HepG2 cells, which endogenously express SYCP3. Western blot analysis showed the successful knockdown of SYCP3 after transfection of small interfering RNA (siRNA) targeting *SYCP3*, with expression levels about half of those in wild-type cells and cells transfected with control non-targeting siRNA (supplementary Fig S5A,B online). We also performed rescue experiments by expressing the siRNA-resistant *FLAG–SYCP3* construct, to confirm the selectivity of the siRNA for the *SYCP3* gene and the specificity of the phenotype. Expression of the exogenous FLAG–SYCP3 protein was not abolished by *SYCP3* siRNA, but the endogenous SYCP3 protein was still successfully knocked down (supplementary Fig S5B online), indicating that the siRNA was selective for the endogenous *SYCP3* mRNA.

The frequency of IR-induced RAD51 foci-positive cells increased from 12.3 ± 0.6% (mean ± s.d.) to 31.3 ± 1.5% after knockdown of SYCP3, but was rescued to 16.7 ± 2.3% when co-transfected with the siRNA-resistant *FLAG–SYCP3* construct (Fig 2E,F). Focusing on cells in S and G2 phases, a robust increase in the frequency of IR-induced RAD51 foci-positive cells from 53.7 ± 2.3% to 94.3 ± 2.5% was observed after silencing SYCP3, which was rescued to 53.3 ± 3.1% in rescue experiments with the siRNA-resistant *FLAG–SYCP3* construct (Fig 2G), confirming the phenotype specificity for the *SYCP3* gene. In contrast, no changes were observed in foci formation of either NBS1 or BRCA1 after knockdown of SYCP3 (supplementary Fig S5C–F online). These observations in siRNA experiments support the results from stable expression of SYCP3 in RPE cells.

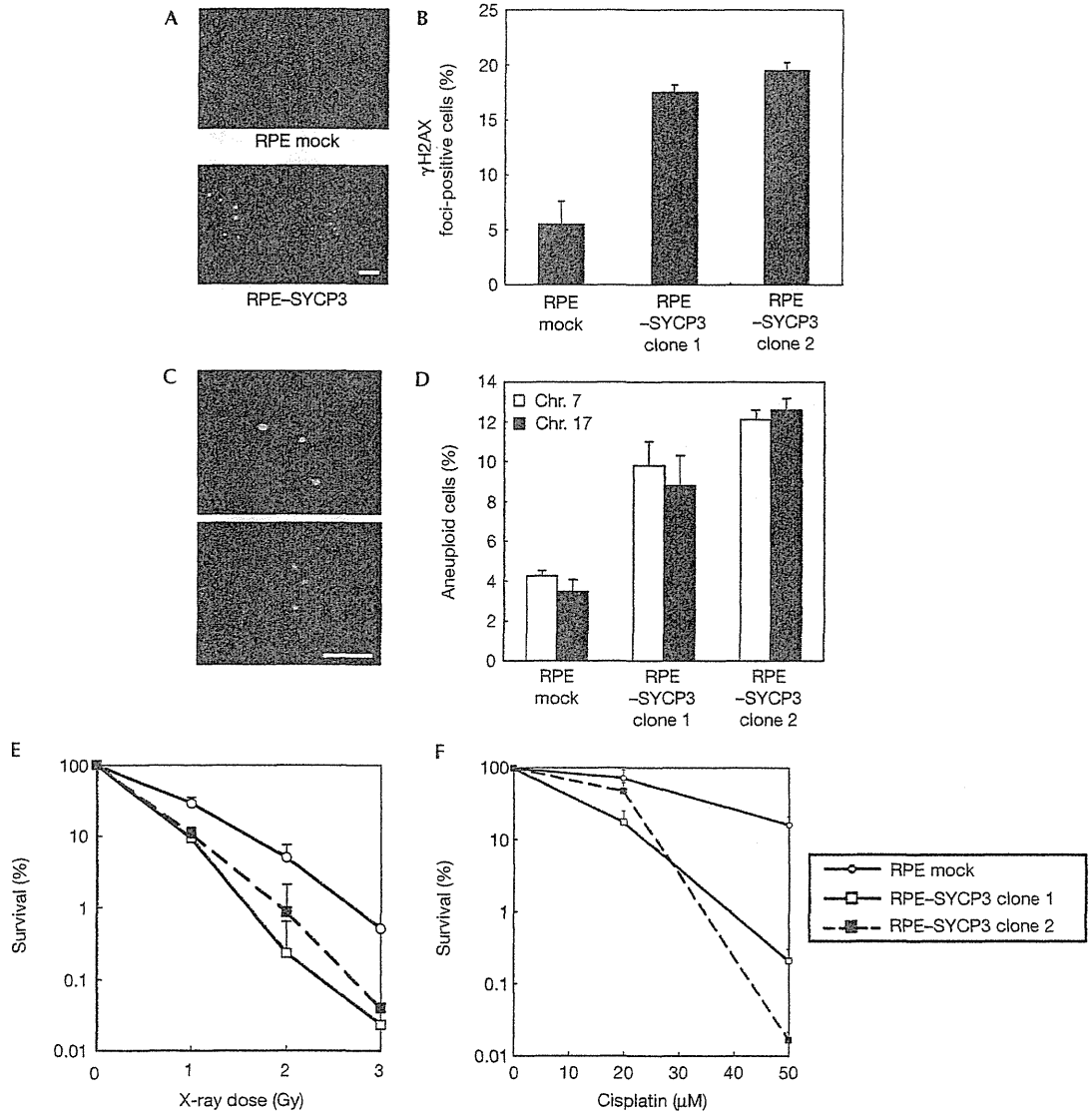

Fig 1 | Expression of SYCP3 leads to increased DNA double-strand breaks (DSBs), aneuploidy and hypersensitivity to DNA-damaging agents. (A) Immunofluorescence visualization of γH2AX foci (green) in RPE cells transfected with an empty vector (upper panel) and in RPE cells expressing SYCP3 (lower panel). Scale bar, 10 μm. (B) Percentage of cells containing more than three large γH2AX foci. A total of 100 cells were examined for each cell clone. (C) Microscopy images of interphase fluorescence *in situ* hybridization in SYCP3-expressing cells using probes for chromosomes 7 (Chr., orange) and 17 (green). Scale bar, 10 μm. (D) Percentage of cells containing one, three or four copies of chromosomes. A total of 500 cells were examined for each cell clone. In B and D, columns and bars represent the mean of three independent experiments and s.d., respectively. (E,F) Sensitivity to ionizing radiation (IR) and cisplatin. The representative result of three independent experiments is shown. The symbols and bars represent mean and s.d. of the triplicate dishes, respectively.

Expression of SYCP3 reduces HR efficiency

Because the results described above indicate that SYCP3 impairs the HR pathway, we next measured the effect of SYCP3 expression on HR efficiency with the DR–green fluorescent protein (GFP) assay (Pierce & Jasin, 2005). First, we stably expressed the exogenous FLAG–SYCP3 protein in HeLa–DRGFP cells (Sakamoto *et al*, 2007; supplementary Fig S6A online), in which GFP-positive cells can be induced on expression of the I-*Sce*I restriction enzyme. Results indicated a significant reduction in the proportion of GFP-positive cells from 8.8 ± 1.2% in mock cells to 4.5 ± 0.7% in FLAG–SYCP3-expressing HeLa–DRGFP cells ($P<0.01$, two-tailed *t*-test; Fig 3A). Second, we established RPE–FLAG–SYCP3 cells in which the DR–GFP reporter system is stably integrated, and found that knockdown of exogenous FLAG–SYCP3 in these cells recovered the proportion of GFP-positive cells from 2.8 ± 0.2% to 5.5 ± 0.9% ($P<0.01$; Fig 3B; supplementary Fig S6B online). Finally, we established HepG2–DRGFP cells and MCF7–DRGFP cells and assessed the effect of knockdown of

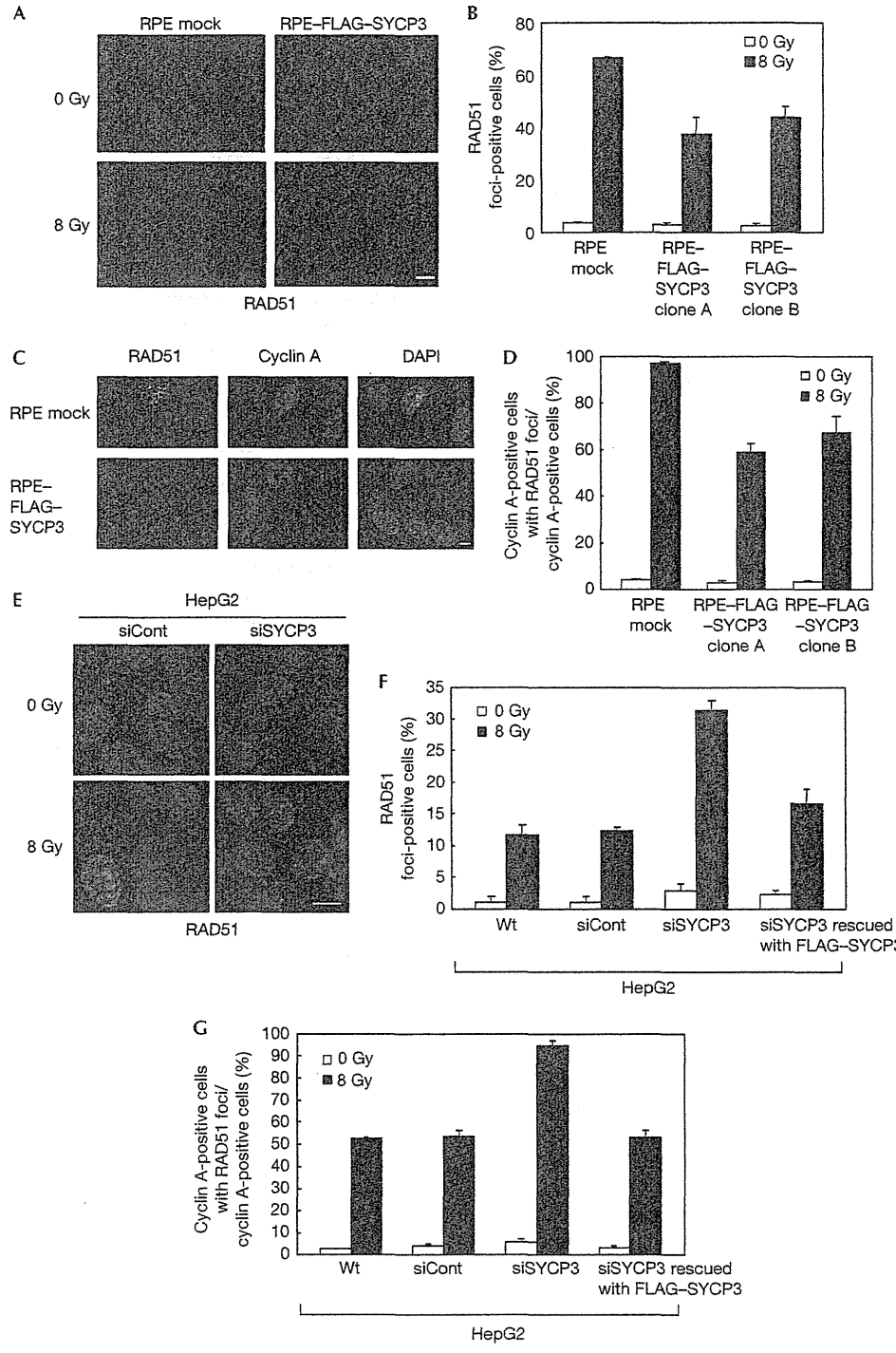

Fig 2 | The mitotic SYCP3 protein inhibits the IR-induced RAD51 foci formation in S and G2 phases. (A,E) Immunofluorescence visualization of RAD51 foci formation (red (A) and green (E)). Cells were non-treated (upper panels) or treated with 8 Gy X-ray (lower panels) and stained at 2 h after irradiation with an anti-RAD51 antibody. Scale bars, 10 μm. (B,F) Percentage of cells containing more than five damage-induced RAD51 foci. (C) Immunofluorescence visualization of RAD51 and cyclin A in RPE cells, showing ionizing radiation (IR)-induced foci formation of RAD51 in RPE-mock cells in S and G2 phases. The cells were treated with 8 Gy X-ray, followed by staining with the anti-RAD51 antibody (green), an anti-cyclin A antibody (red) and DAPI (4,6-diamidino-2-phenylindole; blue) 2 h later. Scale bar, 10 μm. (D,G) Percentage of cells containing more than five IR-induced RAD51 foci in cells stained with cyclin A. In B, D, F and G, columns and bars represent the mean of three independent experiments and s.d., respectively. A total of 100 cells were examined for each cell line. Wt, wild type.

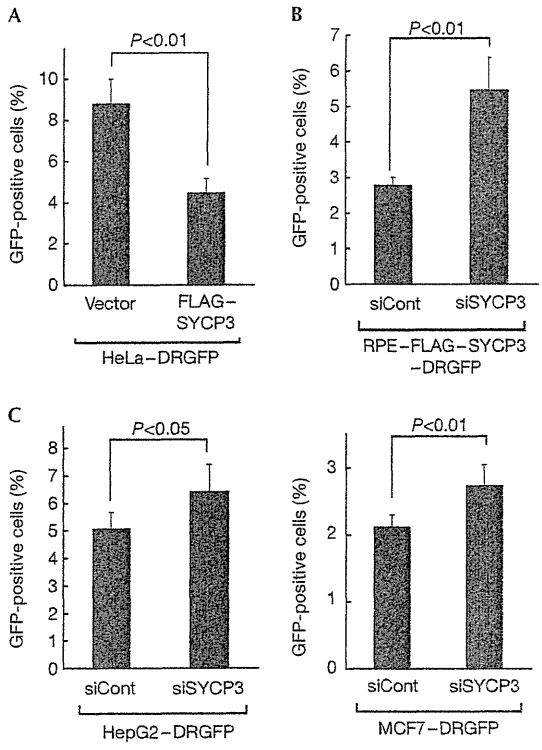

Fig 3 | SYCP3 inhibits the homologous recombination repair activity measured by the DR-GFP assay. (**A**) The proportions of the green fluorescent protein (GFP)-positive cells in HeLa–DRGFP–FLAG–SYCP3 cells and mock cells stably transfected with an empty vector. (**B,C**) The proportions of the GFP-positive cells on knockdown of exogenous FLAG–SYCP3 in RPE–FLAG–SYCP3–DRGFP cells (**B**) or on knockdown of endogenous SYCP3 in HepG2–DRGFP cells and MCF7–DRGFP cells (**C**). In **A**, **B** and **C**, columns and bars represent the mean and s.d. of three independent experiments (**A,B**) or five independent experiments (**C**), respectively.

endogenous SYCP3 in these cells. Silencing endogenous SYCP3 in these cells significantly recovered the proportion of GFP-positive cells from 5.1 ± 0.6% to 6.5 ± 1.0% ($P<0.05$) and from 2.1 ± 0.2% to 2.7 ± 0.3% ($P<0.01$), respectively (Fig 3C; supplementary Fig S6B online). These findings provide direct evidence that SYCP3 reduces the intrinsic HR activity of mitotic cells.

SYCP3 reduces sister chromatid exchanges

A reduction of sister chromatid exchange (SCE) levels is the hallmark of a defect in sister-chromatid-based recombination. A significant reduction in the levels of IR-induced SCE was observed in SYCP3-expressing RPE cells. The frequencies of IR-induced SCEs per cell were 7.7 ± 2.1 in mock cells (mean ± s.d., $n=50$), and 5.8 ± 1.8 and 6.5 ± 2.1 in the two RPE clones expressing SYCP3 ($n=50$) ($P<0.001$, Mann–Whitney U-test). These observations support the findings that SYCP3 impairs the intrinsic HR pathway.

The mitotic SYCP3 protein interferes with BRCA2

To identify the molecule that is targeted by SYCP3, we assessed the localization of the SYCP3 protein and key molecules involved in HR in RPE cells stably expressing FLAG–SYCP3 by immunofluorescence. We found the partial colocalization of FLAG–SYCP3 and BRCA2 in the nucleus (Fig 4A). Moreover, the anti-BRCA2 antibody pulled down FLAG–SYCP3 in these cells (Fig 4B), indicating that SYCP3 forms a complex with BRCA2. The interaction between SYCP3 and BRCA2 was not modified in response to IR-induced DNA damage (Fig 4B).

We next determined whether the DNA damage-induced interaction between BRCA2 and RAD51 is affected by SYCP3 expression. Compared with mock cells, the FLAG–SYCP3-expressing RPE clones showed a reduction in the binding of BRCA2 with RAD51, whereas the protein levels of BRCA2 were not affected (Fig 4C). Conversely, the interaction of these two proteins was recovered by silencing SYCP3 in HT1080 cells, which express SYCP3 endogenously (Fig 4D; supplementary Fig S6C online), confirming that expression of SYCP3 inhibits the interaction between BRCA2 and RAD51 in response to DNA damage.

SYCP3 confers hypersensitivity to a PARP inhibitor

Poly(ADP-ribose) polymerase 1 (PARP1) is a DNA-binding enzyme that is activated by DNA breaks and facilitates the access of base excision/single-strand break repair proteins to the site of damage. Tumours deficient in BRCA1 or BRCA2, which are characterized by defective HR, have been shown to be sensitive to therapies that use PARP inhibitors to achieve synthetic lethality (Bryant *et al*, 2005; Farmer *et al*, 2005).

As our findings showed that SYCP3 expression inhibits the BRCA2 function, we assumed that the mitotic cells expressing SYCP3 would be sensitive to PARP inhibitors. Indeed, RPE cells expressing FLAG–SYCP3 showed extreme hypersensitivity to the PARP inhibitor NU1025, and addition of 4 μM cisplatin markedly enhanced this hypersensitivity (Fig 5A). Conversely, reduced SYCP3 expression levels in HepG2, HT1080 and the breast cancer cell line MCF7 increased the colony survival after treatment with 150 μM NU1025 from 0.9 ± 0.77% (mean ± s.d.) to 7.2 ± 2.2% in HepG2 cells, from 4.0 ± 2.5% to 17.8 ± 2.7% in HT1080 cells and from 7.0 ± 1.5% to 14.0 ± 0.4% in MCF7 cells, respectively (Fig 5B; supplementary Fig S6C online).

The sensitivity to PARP inhibitors in cells that are naturally deficient in BRCA2 should therefore not be affected by SYCP3 expression. The pancreatic cancer cell line Capan1, which expresses endogenous SYCP3 (supplementary Fig S1A online), carries a 6174delT mutation in one BRCA2 allele accompanied by loss of the wild-type allele and is reported to be sensitive to PARP inhibitors (McCabe *et al*, 2005). Supporting this prediction, silencing of SYCP3 in Capan1 cells did not affect the sensitivity to the PARP inhibitor (Fig 5C; supplementary Fig S6C online).

DISCUSSION

Our findings indicate that, in mitotic cells, SYCP3 forms a complex with BRCA2, inhibits the interaction between BRCA2 and RAD51, and impairs the recruitment of RAD51 to resected DSBs, which is a crucial step in the early stages of HR (Fig 5D). This provides a new underlying mechanism for chromosomal instability, in which the function of the BRCA2 tumour suppressor is impaired by the synaptonemal complex protein SYCP3. Importantly, this inhibition of HR might be common in tumours

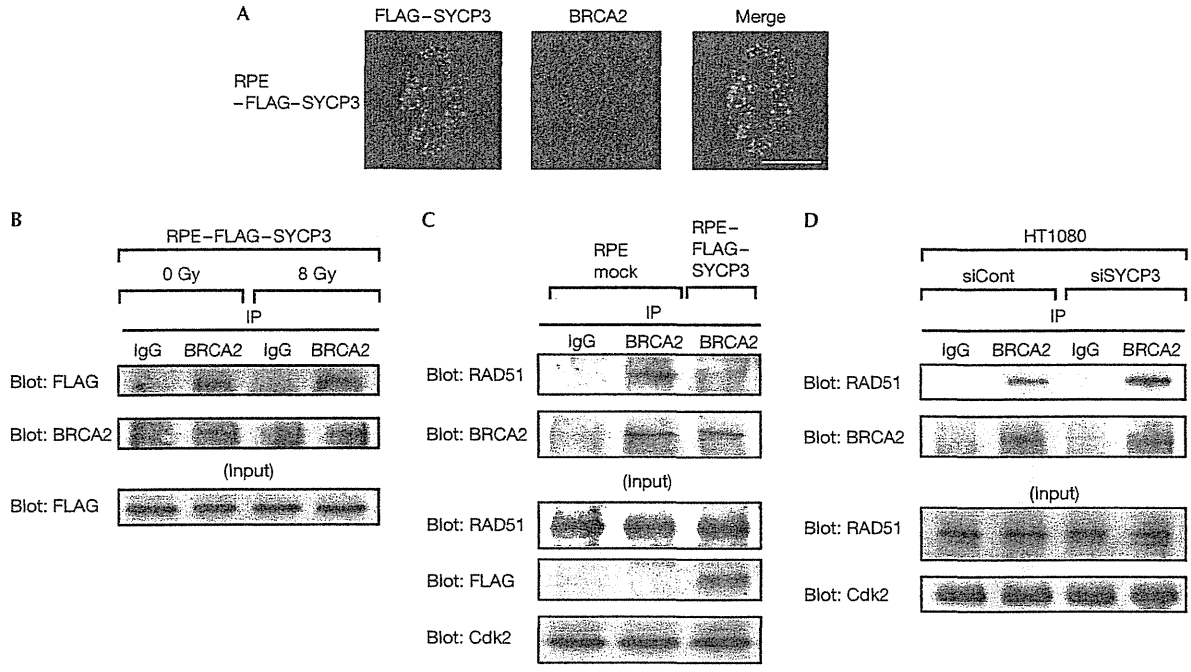

Fig 4 | The mitotic SYCP3 protein interacts with BRCA2 and inhibits interaction between BRCA2 and RAD51 in mitotic cells. (A) Immunofluorescence visualization of FLAG–SYCP3 (left panel) and BRCA2 (middle panel). Cells were stained with anti-FLAG (green) and anti-BRCA2 (red) antibodies and 4,6-diamidino-2-phenylindole (blue), and merged (right panel). Scale bar, 10 μm. (B) Association of FLAG–SYCP3 with BRCA2 in FLAG–SYCP3-expressing RPE cells unirradiated or irradiated with 8 Gy X-ray 2 h before collecting the cell lysates. (C) Coimmunoprecipitation of BRCA2 with RAD51 from lysates of mock cells and RPE cells stably expressing FLAG–SYCP3 collected 3 h after inducing DNA damage by treatment with 50 μM cisplatin for 1 h. (D) Coimmunoprecipitation of BRCA2 with RAD51 from lysates of HT1080 cells transfected with a non-targeting small interfering RNA (siRNA) control or siRNA for *SYCP3*. In B, C and D, 500 μg of total cell lysates was precipitated using the anti-BRCA2 antibody or normal mouse immunoglobulin G (IgG) as a negative control and visualized by western blotting using the anti-FLAG antibody (B, upper panel), the anti-RAD51 antibody (C,D, upper panel) or the anti-BRCA2 antibody (lower panels). IP, immunoprecipitation.

of various tissue origins, as well as in breast and ovarian cancers with no detected *BRCA2* mutations, because SYCP3 is expressed in various tumours.

The BRCA2-interacting proteins have a crucial role in modulating the HR pathway. In contrast to the previously identified proteins such as PALB2, BCCIP and DSS1, which promote the BRCA2–RAD51 repair machinery (Gudmundsdottir *et al*, 2004; Lu *et al*, 2005; Oliver *et al*, 2009), SYCP3 is a new type because it inhibits the repair pathway. Although our preliminary data showed a direct association between SYCP3 and full-length BRCA2 (data not shown), further characterization of the interaction between SYCP3 and BRCA2 would be needed to address how SYCP3 interacts with BRCA2 and how it inhibits the binding of RAD51 to BRCA2.

Finally, our findings provide a new insight in therapeutic strategies for cancer. Tumours with aberrant SYCP3 expression should show a satisfactory response to radiotherapy, cisplatin-based chemotherapy and especially PARP inhibitors. Although clinical studies indicated that PARP inhibitors are highly effective for cancers with *BRCA1* or *BRCA2* mutation (Fong *et al*, 2009), our finding that SYCP3 expression confers extreme hypersensitivity to PARP inhibitors would be applied to a broader range of tumours expressing SYCP3, including cancers with no detected *BRCA1* or *BRCA2* mutations. Establishment of this new therapeutic strategy would require further analyses in large patient cohorts and tumour models.

METHODS

Cell lines, samples, antibodies, expression analysis and vector constructions. Detailed descriptions are provided in the supplementary information online.

Stable expression of *SYCP3* cDNA in mitotic cells. The expression vectors for *SYCP3* or *FLAG–SYCP3* were transfected at 1,200 V and 10 μF into RPE cells and at 250 V and 950 μF into HeLa–DRGFP cells using the Bio-Rad Gene Pulser II. Stable clones were selected with 900 μg ml^{-1} Zeocin (Invitrogen).

siRNA. The siRNA targeting the 3′ untranslated region of *SYCP3* mRNA (5′-GCUUUCAGCUCUUUAGUAAUGAUAG-3′) was synthesized by Invitrogen and used to knock down endogenous SYCP3. To knock down exogenous FLAG–SYCP3, the predesigned siRNA (AM16704) from Ambion was used. An siCONTROL non-targeting siRNA from Dharmacon was used as a control. For transfection of the siRNA, see supplementary information online.

Immunoprecipitation, immunofluorescence, fluorescence *in situ* hybridization analysis, cell survival assays, analysis of SCEs and cell cycle analysis. Detailed protocols are provided in the supplementary information online.

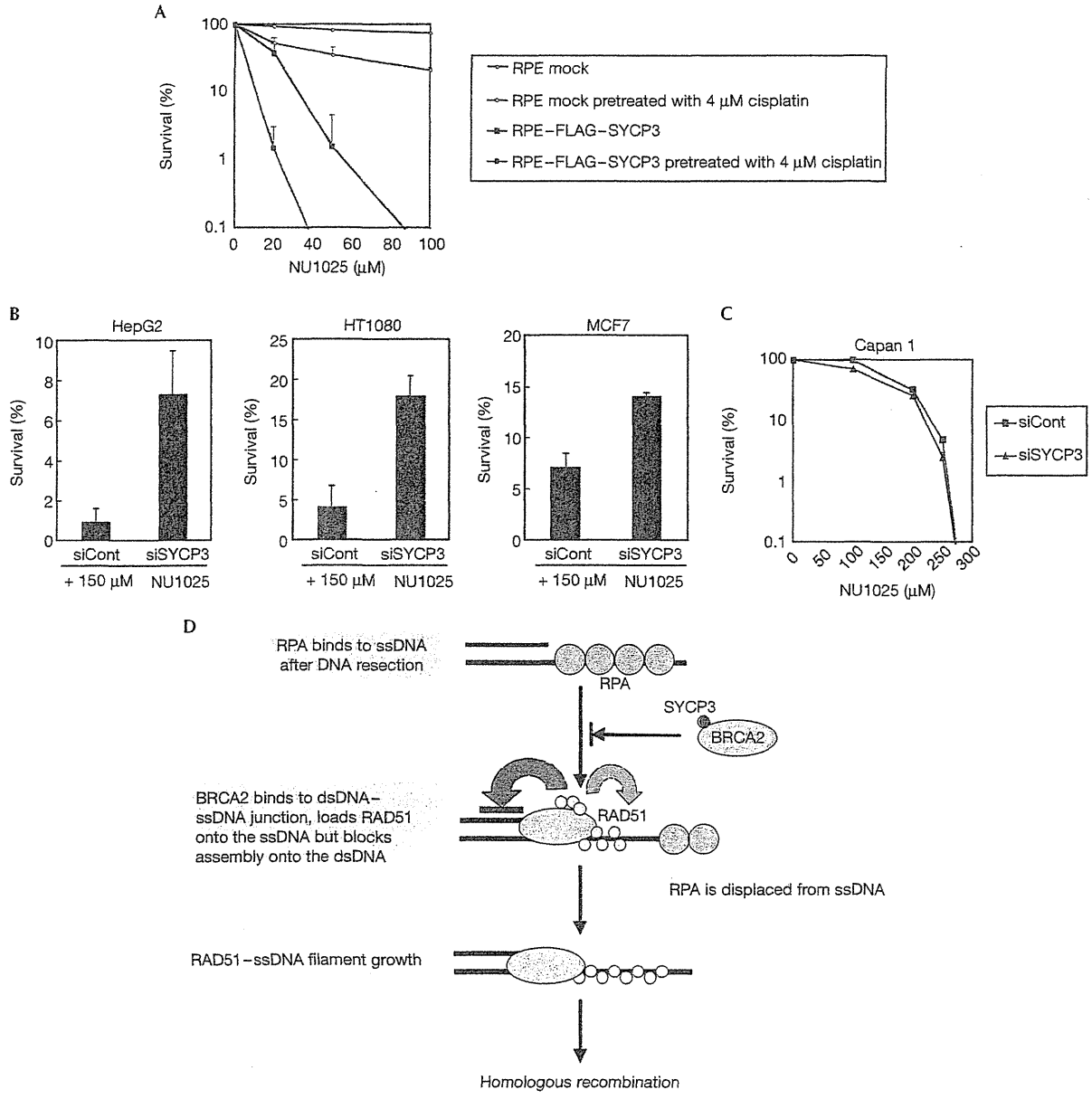

Fig 5 | SYCP3 impairs the BRCA2 recombination mediator activity in mitotic cells and hypersensitizes the cells to the inhibitor of PARP. (A) Colony outgrowth of the RPE cells expressing or not expressing FLAG–SYCP3 either untreated or treated with 4 μM cisplatin for 1 h before continuous exposure to the poly(ADP-ribose) polymerase (PARP) inhibitor NU1025. The representative result of three independent experiments is shown. The mean and s.d. of the triplicate dishes are indicated. (B,C) Colony survival of HepG2 cells (B), HT1080 cells (B), MCF7 cells (B) and Capan1 cells (C) transfected with SYCP3-targeting small interfering RNA (siRNA) and a non-targeting siRNA control after continuous treatment with NU1025. Columns and bars represent the mean of three independent experiments and s.d., respectively. (D) A proposed model for inhibition of RAD51-dependent homologous recombination by SYCP3. BRCA2 binds to the double-stranded DNA (dsDNA)–single-stranded DNA (ssDNA) junction and loads RAD51 onto ssDNA while suppressing RAD51–dsDNA binding. SYCP3 impairs the recruitment of RAD51 to resected DSBs by forming a complex with BRCA2.

The DR–GFP assay. Stable integrants were obtained by transfecting the RPE–FLAG–SYCP3 cells, MCF7 cells and HepG2 cells with the linearized phprtDR–GFP construct and selecting with puromycin as described previously (Sakamoto *et al*, 2007). For more details, see supplementary information online.

Supplementary information is available at EMBO *reports* online (http://www.emboreports.org).

ACKNOWLEDGEMENTS

We are grateful to Maria Jasin for the DR–GFP construct and the I-*Sce*I expression plasmid, and Kenshi Komatsu and Junya Kobayashi for providing us with HeLa–DRGFP cells. We also thank Eri Nagata and Hidekazu Suzuki for their technical assistance. This work was supported in part by Grants-in-Aid for Scientific Research from the Japan Society for the Promotion of Science to K.M. and to N.H., by SHISEIDO Grants for Women Scientists to N.H. and by the Itoe Okamoto Scientific Award, SHISEIKAI, to N.H.

Author contributions: N.H. performed most of the experiments. M.O., A.K., Y.F., T.H. and J.S. assisted with the experiments. N.H., S.T. and K.M. analysed data. N.H. and K.M. wrote the paper.

CONFLICT OF INTEREST

The authors declare that they have no conflict of interest.

REFERENCES

Bryant HE, Schultz N, Thomas HD, Parker KM, Flower D, Lopez E, Kyle S, Meuth M, Curtin NJ, Helleday T (2005) Specific killing of BRCA2-deficient tumours with inhibitors of poly(ADP-ribose) polymerase. *Nature* **434:** 913–917

Farmer H *et al* (2005) Targeting the DNA repair defect in BRCA mutant cells as a therapeutic strategy. *Nature* **434:** 917–921

Fong PC *et al* (2009) Inhibition of poly(ADP-ribose) polymerase in tumors from BRCA mutation carriers. *N Engl J Med* **361:** 123–134

Gudmundsdottir K, Ashworth A (2006) The roles of BRCA1 and BRCA2 and associated proteins in the maintenance of genomic stability. *Oncogene* **25:** 5864–5874

Gudmundsdottir K, Lord CJ, Witt E, Tutt AN, Ashworth A (2004) DSS1 is required for RAD51 focus formation and genomic stability in mammalian cells. *EMBO Rep* **5:** 989–993

Hartlerode AJ, Scully R (2009) Mechanisms of double-strand break repair in somatic mammalian cells. *Biochem J* **423:** 157–168

Kang TH, Noh KH, Kim JH, Bae HC, Lin KY, Monie A, Pai SI, Hung CF, Wu TC, Kim TW (2010) Ectopic expression of X-linked lymphocyte-regulated protein pM1 renders tumor cells resistant to antitumor immunity. *Cancer Res* **70:** 3062–3070

Lu H, Guo X, Meng X, Liu J, Allen C, Wray J, Nickoloff JA, Shen Z (2005) The BRCA2-interacting protein BCCIP functions in RAD51 and BRCA2 focus formation and homologous recombinational repair. *Mol Cell Biol* **25:** 1949–1957

Maatouk DM, Kellam LD, Mann MR, Lei H, Li E, Bartolomei MS, Resnick JL (2006) DNA methylation is a primary mechanism for silencing postmigratory primordial germ cell genes in both germ cell and somatic cell lineages. *Development* **133:** 3411–3418

McCabe N, Lord CJ, Tutt AN, Martin NM, Smith GC, Ashworth A (2005) BRCA2-deficient CAPAN-1 cells are extremely sensitive to the inhibition of poly (ADP-ribose) polymerase: an issue of potency. *Cancer Biol Ther* **4:** 934–936

Niemeyer P, Tureci O, Eberle T, Graf N, Pfreundschuh M, Sahin U (2003) Expression of serologically identified tumor antigens in acute leukemias. *Leuk Res* **27:** 655–660

Nojima K *et al* (2005) Multiple repair pathways mediate tolerance to chemotherapeutic cross-linking agents in vertebrate cells. *Cancer Res* **65:** 11704–11711

Oliver AW, Swift S, Lord CJ, Ashworth A, Pearl LH (2009) Structural basis for recruitment of BRCA2 by PALB2. *EMBO Rep* **10:** 990–996

Page SL, Hawley RS (2004) The genetics and molecular biology of the synaptonemal complex. *Annu Rev Cell Dev Biol* **20:** 525–558

Pierce AJ, Jasin M (2005) Measuring recombination proficiency in mouse embryonic stem cells. *Methods Mol Biol* **291:** 373–384

Sakamoto S, Iijima K, Mochizuki D, Nakamura K, Teshigawara K, Kobayashi J, Matsuura S, Tauchi H, Komatsu K (2007) Homologous recombination repair is regulated by domains at the N- and C-terminus of NBS1 and is dissociated with ATM functions. *Oncogene* **26:** 6002–6009

Simpson AJ, Caballero OL, Jungbluth A, Chen YT, Old LJ (2005) Cancer/testis antigens, gametogenesis and cancer. *Nat Rev Cancer* **5:** 615–625

Tashiro S, Walter J, Shinohara A, Kamada N, Cremer T (2000) Rad51 accumulation at sites of DNA damage and in postreplicative chromatin. *J Cell Biol* **150:** 283–291

Free Radical Biology & Medicine 52 (2012) 507–515

Contents lists available at SciVerse ScienceDirect

Free Radical Biology & Medicine

journal homepage: www.elsevier.com/locate/freeradbiomed

Original Contribution

Serine-Threonine Kinase 38 is regulated by Glycogen Synthase Kinase-3 and modulates oxidative stress-induced cell death

Atsushi Enomoto [a,*], Naoki Kido [a], Michihiko Ito [b], Nobuhiko Takamatsu [b], Kiyoshi Miyagawa [a]

[a] Laboratory of Molecular Radiology, Center for Disease Biology and Integrative Medicine, Graduate School of Medicine, The University of Tokyo, 7-3-1 Hongo, Bunkyo-ku Tokyo 113-0033, Japan

[b] Department of Biosciences, School of Science, Kitasato University, 1-15-1 Kitasato, Sagamihara, Kanagawa 252-0373, Japan

ARTICLE INFO

Article history:
Received 27 May 2011
Revised 20 October 2011
Accepted 5 November 2011
Available online 13 November 2011

Keywords:
STK38
GSK-3
Phosphorylation
Oxidative stress
JNK
Free radicals

ABSTRACT

Serine-threonine kinase 38 (STK38) is a member of the protein kinase A (PKA)/PKG/PKC-like family. In the present study, we investigated the regulatory mechanism of STK38 and assessed its role in the cellular stress response. Among various environmental stresses, STK38 was specifically activated by H_2O_2, and the phosphatidylinositol 3-kinase inhibitor wortmannin or AKT inhibitor IV suppressed this activation. STK38 was also activated by a constitutively active AKT1 or by GSK-3β inhibitor VII. The phosphorylation level of GSK-3β was correlated with the STK38 activity, in response to various stimuli and in different cell lines. Co-immunoprecipitation analysis revealed that GSK-3β physically interacted with STK38 in cells. GSK-3β overexpression inhibited the H_2O_2-stimulated STK38 activity. GSK-3β phosphorylated STK38 on residues S6 and T7 *in vitro*, depending largely on a PKA-mediated priming phosphorylation of STK38 on residues S10 and S11, respectively. STK38's H_2O_2-stimulated activity was enhanced by alanine substitution at its priming sites and/or at S6 and T7, and it was partially reduced by a phosphomimetic mutation at S6 or T7. STK38 knockdown enhanced the H_2O_2-induced JNK phosphorylation and cell death. Our results indicate that that GSK-3β inhibits STK38's full activation, and suggest that STK38 activation is required to prevent cell death in response to oxidative stress.

Introduction

STK38 (Serine-Threonine Kinase 38, also known as NDR1; Nuclear Dbf-2 Related 1, GenBank accession number NP009202) is a serine/threonine protein kinase belonging to a subclass of the protein kinase A (PKA)/PKG/PKC-like (AGC) family [1-3], which includes cAMP-dependent kinase, protein kinase B, and protein kinase C. The members of the STK38 family comprise *Drosophila melanogaster* TRC, *Schizosaccharomyces pombe* Orb6, *Saccharomyces cerevisiae* Cbk1 and Dbf2, the mammalian STK38, STK38L, LATS1 (Large tumor suppressor-1), and LATS2 [1-3]. Of these, Cbk1 and Orb6 are involved in regulating cell morphology [4,5], and Dbf2 is a cell cycle-regulated kinase whose activity is required for progression through anaphase [6]. In mammals, LATS1/2 function as tumor suppressors, whereas STK38 and STK38L may function as proto-oncogenes [3]. Recently, STK38 was implicated in centrosome duplication [7], and we previously reported that STK38 interacts with the JNK kinase kinases MEKK1/2, and negatively regulates their signaling pathways [8].

STK38 and its relatives have a conserved N-terminal regulatory domain (NTR), a catalytic kinase domain containing the activation segment phosphorylation site, and a C-terminal regulatory domain [3]. The N-terminal regulatory region of the STK38 family includes a number of conserved basic hydrophobic residues and is predicted to form an amphiphilic α-helix. The C-terminal regulatory domain of the STK38 family protein kinases contains a hydrophobic motif that houses phosphorylation sites. As with many AGC kinases, STK38 is phosphorylated on two conserved residues, one in the activation loop of the catalytic domain and one in the C-terminal hydrophobic domain [9]. Phosphorylation of both residues is essential for the full activation of STK38 [10,11]. One protein kinase, mammalian STE20-like kinase 3 (MST3), has been shown to specifically phosphorylate only the hydrophobic motif of STK38s, but not the activation segment [11]. Otherwise, how STK38 is regulated by upstream kinases is largely unknown.

In this study, we show that STK38 is activated by H_2O_2 and provide genetic, enzymatic, and pharmacological evidence that STK38 is regulated by GSK-3β. Moreover, we describe the role of STK38 in H_2O_2-induced cell death.

Abbreviations: STK38, Serine Threonine Kinase 38; NDR, Nuclear Dbf-2 Related; GSK-3, Glycogen Synthase Kinase-3; PKA, Protein Kinase A; CA-AKT1, Constitutive active AKT1; NTR domain, N-terminal regulatory domain.

* Corresponding author. Fax: +81 3 5841 3013.
E-mail address: aenomoto-tky@umin.ac.jp (A. Enomoto).

0891-5849/$ – see front matter © 2011 Elsevier Inc. All rights reserved.
doi:10.1016/j.freeradbiomed.2011.11.006

Materials and methods

Cell culture, stimulation, transfection, and cell viability

HEK293T, COS-7, Hs27, MCF-7, and HeLa cells were cultured in Dulbecco's modified Eagle's medium/F-12 (1:1) (Sigma, St. Louis, MO, USA) supplemented with 10% fetal bovine serum (Hyclone, South Logan, UT, USA) and 1% penicillin/streptomycin (Sigma). MKN45 and LU99 cells were cultured in RPMI 1640 (Sigma) supplemented with 10% fetal bovine serum and 1% penicillin/streptomycin. The cells were either untreated or were pretreated with wortmannin (Sigma), KU-55933 (Calbiochem, Darmstadt, Germany), or AKT inhibitor IV (Calbiochem) for 30–60 min, and then stimulated for the indicated times with etoposide (Sigma), D-sorbitol (Sigma), anisomycin (Sigma), GSK-3β inhibitor VII, (Calbiochem), or H_2O_2 (Wako Pure Chemical Industries, Osaka, JAPAN).

For the transient transfection assays, the cells were plated on 60- or 100-mm dishes 24 h before the transfection, and transfected for 24–48 h with the appropriate expression vectors using FuGENE HD (Roche, Indianapolis, IN, USA). Empty pcDNA 3.1 vector was used to keep the total amount of DNA equivalent for each transfection. For the cell viability assay, HeLa cells were transiently transfected with either a non-targeting or an *stk38*-specific shRNA expression vector. Twenty-four hours after the transfection, the cells were washed twice with Ca^{2+}/Mg^{2+}-free phosphate buffered saline (PBS^-) and then cultured in medium containing 2 μg/ml puromycin (Invivogen, San Diego, CA, USA) for 48 hours. The cells were washed twice with PBS^-, and either left untreated or treated with 100 μM H_2O_2 for 16 hours, then assayed for viability. Cell viability was determined by Annexin V–FITC and propidium iodide (PI) staining using a MEBCYTO Apoptosis kit (MBL, Nagoya, Japan). The Annexin V-PI staining can be used in a bivariate analysis to distinguish between cells undergoing apoptosis (PI negative) and those that are necrotic or dead (PI positive). Cell death was defined as the total percentage of PI-positive and/or Annexin V-positive cells. All samples were counted, and over 5000 cells for each condition were analyzed on a flow cytometer (EPICS XL System II, Beckman Coulter, Brea, CA, USA).

Antibodies

A polyclonal antibody against human STK38 was described previously [8]. The anti-phospho-AKT (Ser473), anti-phospho-β-Catenin (Ser33/37/Thr41), anti-β-Catenin, and anti-phospho-GSK-3β (Ser9) antibodies were purchased from Cell Signaling Technology (Beverly, MA, USA). The anti-NDR1 antibody was obtained from Santa Cruz Biotechnology (Santa Cruz, CA, USA). The anti-GSK-3 and anti-AKT1/PKBα antibodies were from Upstate Cell Signaling Solutions (Lake Placid, NY, USA). The anti-V5 antibody and anti-phospho-GSK-3β (Ser9) were from MBL or Epitomics (Burlingame, CA, USA), respectively. Anti-Xpress was from Invitrogen (Carlsbad, CA, USA).

Western blotting analysis

Western blotting analyses were performed as described previously [12]. The amounts of phospho-GSK-3 s or phospho-JNKs were quantified using a luminescent image analyzer, LAS-1000 mini (Fuji Film, Tokyo, Japan).

Plasmids

The mammalian expression vectors pcD3.1-V5 STK38, pcD3.1-V5 STK38 (K118A), and pcDNA3.1-V5 ΔN STK38, were previously described [8]. The constitutively active AKT1/PKBα vector was purchased from Millipore. The STK38 mutants (ΔN2 (12–466), S6A, S6A/K118A, T7A, T7A/K118A, S6A/T7A, S10A/S11A, and S6A/T7A/S10A/S11A: 4×A) were generated by PCR-based mutagenesis. Each of the PCR products was subcloned into the pcDNA3.1-V5 TOPO TA expression vector (Invitrogen, Carlsbad, CA, USA). The GSK-3β (S9A) mutant was generated by PCR-based mutagenesis and subcloned into the pcD4/His-Max topo TA expression vector (Invitrogen). For bacterial expression, the region encoding residues 1–121 of STK38, termed NT-STK38, and the NT-STK38 mutants (S6A, T7A, S6A/T7A, S10A/S11A) were amplified by PCR using pcD3.1-V5 STK38 (K118A) as the template. Each PCR fragment was subcloned into the pBAD/TOPO ThioFusion-His-V5 expression vector (Invitrogen). The mammalian STK38 short hairpin (sh) RNA expression vector was described previously [8]. All constructs were confirmed by sequencing.

Bacterial expression of His-tagged STK38 variants

The Top10 *Escherichia coli* strain (Invitrogen) was transformed with the pBAD/TOPO ThioFusion-His-NT-STK38 mutant expression vector. Mid-logarithmic phase cells were induced with 0.002% arabinose (Sigma) for 6 h at 20 °C. Cell lysates were prepared with B-PER bacterial protein extraction reagents (Pierce, Rockford, IL, USA) containing protease inhibitors, and the fusion proteins were purified under native conditions with Ni-NTA agarose (Qiagen, Hilden, Germany). Each of the recombinant proteins was used as a substrate for the GSK3 kinase assay as described below.

Immunoprecipitation and immune complex kinase assays

Cell lysates were prepared as described [8]. The cell lysates were incubated with a specific antibody and then mixed with protein A/G agarose. For binding assays, the immunocomplexes were washed three times with lysis buffer, and subjected to Western blotting analysis. For immune complex kinase assays, the immunoprecipitates were rinsed three times with lysis buffer and then twice with kinase buffer. In brief, for GSK-3 kinase assay, the recombinant NT-STK38 mutants or immunopurified STK38 mutants were pre-treated or not with 250 U of recombinant PKA (New England BioLabs, Ipswich, MA, USA) in PKA kinase buffer (50 mM Tris–HCl (pH 7.5), 10 mM $MgCl_2$) containing unlabeled ATP at 30 °C for 30 min. The beads were then washed four times with TNE buffer and twice with GSK-3 kinase buffer (20 mM Tris–HCl (pH 7.5), 10 mM $MgCl_2$, 5 mM DTT). GSK-3 kinase reactions were initiated by the addition of 100 U of GSK-3β (New England BioLabs) to the beads in GSK-3 kinase buffer containing 0.37 MBq ml^{-1} [γ-^{32}P] ATP. After 30 minutes at 30 °C, the kinase reactions were stopped by the addition of 2×SDS sample buffer. For the AKT1 kinase assay, recombinant active AKT1 (0.25 μg; Millipore) was treated alone or with 1.0 μg of recombinant SEK1 (K129R) or STK38 (K118A) in 30 μl of AKT kinase buffer (20 mM Tris–HCl (pH 7.5), 20 mM $MgCl_2$) containing 0.37 MBq ml^{-1} [γ-^{32}P] ATP. After 30 minutes at 30 °C, the kinase reactions were stopped by the addition of 2×SDS sample buffer. The reaction products were subjected to SDS-PAGE and analyzed with a phosphoimaging device (BAS-2500; Fuji Film). Measurement of STK38 kinase activity was as described previously [8].

Results

Activation of STK38 by H_2O_2

We previously reported that STK38 negatively regulates the JNK kinase kinases, MEKK1/2 [8]. To clarify how STK38 is regulated, we transiently transfected HEK 293 T cells with V5-tagged STK38, and then examined the STK38 activity in response to various extracellular stresses that are known to activate JNK signaling [13], using an immune complex kinase assay. The kinase activity of immunoprecipitated V5-STK38 was significantly stimulated (2.9-fold) by treatment with H_2O_2, but treatment with etoposide, sorbitol, or anisomycin had no effect. (Fig. 1A). The negative control cells, expressing a kinase-dead mutant of STK38 (K118A), displayed a reduced basal

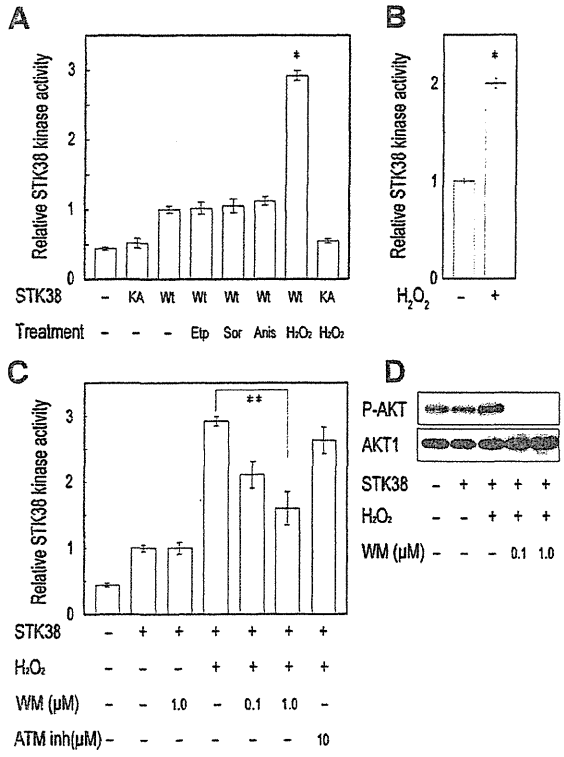

Fig. 1. H_2O_2-induced STK38 activation and its inhibition by wortmannin. (A) Effect of various stimuli on STK38 activity. HEK293T cells were transiently transfected with an empty vector or mammalian expression vector encoding Wild-type (Wt) STK38-V5 or kinase-dead mutant STK38 K118A (KA)-V5. Forty-eight hours after transfection, the cells were exposed to etoposide (50 μM for 1 h), anisomycin (0.2 μg/ml for 30 min), sorbitol (0.2 M for 30 min), or H_2O_2 (2 mM for 30 min). Cell lysates were prepared and the STK38 kinase activity was measured by immune complex kinase assay with an anti-V5 antibody, using a synthetic peptide as the substrate. STK38 activity was measured with a liquid scintillation counter. (B) Endogenous STK38 is activated by treatment with H_2O_2. HeLa cells were treated with H_2O_2 (2 mM for 30 min) or left untreated. The cell lysates were prepared and subjected to an STK38 kinase assay. (C) Wortmannin inhibits H_2O_2-induced STK38 activation. Transfected cells were stimulated with H_2O_2 (2 mM for 30 min) after pretreatment with DMSO, wortmannin, or ATM inhibitor at the indicated dose for 30 min. Cell lysates were prepared, and the STK38 kinase activity was measured as described above. (D) Wortmannin inhibits H_2O_2-induced AKT phosphorylation. The endogenous AKT expression levels and phosphorylation were analyzed by Western blotting. Data represent the average and standard deviations of five independent experiments, expressed as the STK38 kinase activity relative to that of cells expressing wild-type STK38 without stimulation. Statistical analysis was performed using the Student's *t*-test. *, $p<0.05$ when compared with the wild type without stimulation was considered significant. **, $p<0.05$ when compared with the H_2O_2-treated wild type was considered significant.

kinase activity that was not stimulated by H_2O_2. Exposing HeLa cells to H_2O_2 increased the endogenous STK38 kinase activity 2.0-fold (Fig. 1B and Supplemental Fig. 1A). Pre-treatment with a phosphatidylinositol 3-kinase (PI-3 K) inhibitor, wortmannin, blocked the H_2O_2-stimulated STK38 activation in a dose-dependent manner (Fig. 1C). We also examined a member of the PI-3 K family, ataxia telangiectasia mutated (ATM), for its ability to activate STK38. However, the ATM-specific inhibitor KU-55933 had little or no effect on the H_2O_2-stimulated STK38 activity. We also confirmed that H_2O_2 enhanced AKT phosphorylation in our system, (Fig. 1D and Supplemental Fig. 1B), and that wortmannin inhibited this phosphorylation (Fig. 1D). These results suggested that the PI-3 K-AKT pathway might be involved in regulating STK38.

Activation of STK38 by AKT

We next examined the influence of AKT activation on the H_2O_2-stimulated STK38 activity. HeLa cells were pre-treated with AKT inhibitor IV, and then treated with H_2O_2. The endogenous STK38 protein was then immunoprecipitated from the cell extracts and subjected to the immune complex kinase assay. As shown in Fig. 2A, AKT inhibitor IV significantly blocked the H_2O_2-stimulated STK38 activation. We next transiently expressed STK38-V5 in HEK293T cells with or without a constitutively active myristoylated AKT1 (CA-AKT1), and subjected the STK38-V5 protein immunoprecipitated from the cell extracts to the immune complex kinase assay. CA-AKT1 overexpression stimulated the STK38 activity 2.1-fold, but did not stimulate the activity of the kinase-dead mutant STK38 (K118A) (Fig. 2B). These results suggested that AKT activation is important for stimulating the STK38 activity.

To determine whether AKT could phosphorylate STK38 directly, we performed an *in vitro* AKT kinase assay. AKT1 phosphorylated SEK1 (K129R), as previously reported (Fig. 2C, lane 5) [14]. However, recombinant AKT1 did not phosphorylate STK38 (K118A), indicating that STK38 is not an AKT substrate (Fig. 2C, lane 4). Interestingly, when co-expressed with CA-AKT1 in HEK293T cells, STK38 migrated as two forms, a major, slower-migrating form and a barely detectable

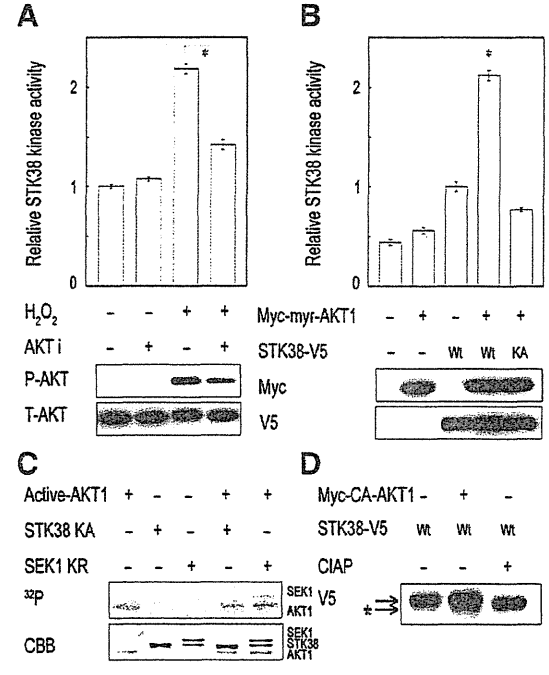

Fig. 2. STK38 activity is stimulated through activation of the AKT pathway. (A) H_2O_2-induced STK38 activation is AKT-dependent. HeLa cells were left untreated or treated with 2.5 μM AKT inhibitor IV (AKTi) for 1 h, and then treated with 2 mM H_2O_2 for 20 min. Cell lysates were prepared and subjected to an STK38 kinase assay. Data represent the average and standard deviation of three independent experiments. Statistical difference between H_2O_2–treated cells with vehicle (DMSO) and AKT inhibitor IV is indicated by an astersik (*, $p<0.05$). (B) HEK293T cells were transiently transfected with an empty vector or mammalian expression vector encoding either V5-tagged wild-type (Wt) STK38 or kinase-dead mutant STK38 K118A (KA) with or without the Myc-tagged constitutively active myristoylated-AKT1 (CA-AKT1) expression vector. Forty-eight hours after transfection, the V5-tagged STK38 was immunopurified using the anti-V5 antibody, and the STK38 kinase activity was assessed by an *in vitro* kinase assay. Data represent the average and standard deviation of three independent experiments. *, $p<0.05$ when compared with the cells expressing only wild type STK38 was considered significant. Total cell lysates were analyzed for the amount of V5-tagged STK38 or Myc-tagged AKT1 by Western blotting. (C) STK38 is not a target of AKT. Purified His-STK38 (K118A) or GST-SEK1 (K129R) was incubated with kinase buffer alone (lane 2 or 3) or active AKT1 (lane 4 or 5). As a control, active AKT1 was incubated in the kinase buffer alone containing [γ-^{32}P] ATP (lane 1). Proteins were separated by SDS-PAGE and visualized by either autoradiography (upper panel) or Coomassie Brilliant Blue staining (lower panel). (D) Cell lysates were treated with or without calf intestine alkaline phosphatase (CIAP) at 30 °C for 30 min, then subjected to Western blotting analysis with the anti-V5 antibody. In the presence of CA-AKT1, wild-type STK38 usually displayed two bands (arrows): a main, slower-migrating form and a barely detectable faster-migrating form. The asterisk illustrates the latter form.

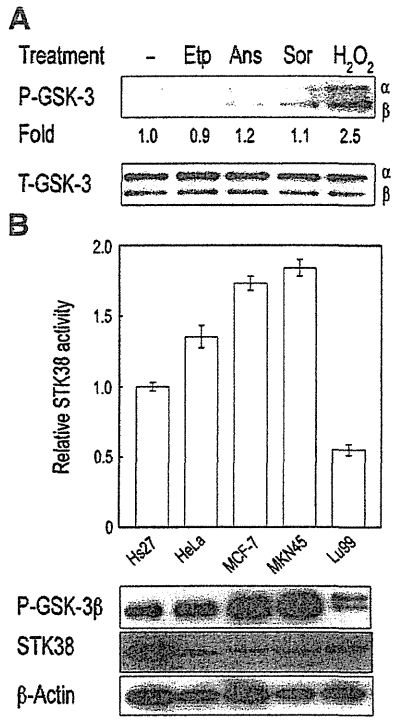

Fig. 3. GSK-3 phosphorylation levels correlate with STK38 activity. (A) Phosphorylation of GSK-3 is enhanced by H_2O_2. HEK293T cells were treated as described in Fig. 1A and harvested. The cell lysates were subjected to Western blotting analysis using the indicated antibodies. (B) Subconfluent proliferating cultures of one normal foreskin fibroblast cell line (Hs27) and four cancer cell lines (epithelioid carcinoma HeLa, mammary gland adenocarcinoma MCF-7, stomach adenocarcinoma MKN45, and lung giant cell carcinoma LU99) were harvested and lysed. The STK38 kinase activity was assessed by an *in vitro* kinase assay of STK38 immunopurified from each cell line. Data represent the average and standard deviations of three independent experiments, expressed as the STK38 kinase activity relative to that in the normal cell line Hs27 without stimulation. Endogenous GSK-3β phosphorylation levels and endogenous β-Actin or STK38 expression levels in the total cell lysates were analyzed by Western blotting with the indicated antibodies.

faster-migrating form (Fig. 2D, lane 2). When treated with a protein phosphatase, the migration of STK38 was also more rapid than that of untreated STK38 (Fig. 2D, lane 3). These results suggest that the slower-migrating form of STK38 consisted of phosphorylated species, and the faster-migrating one consisted of non-phosphorylated or hypo-phosphorylated species. These findings suggest that AKT1 induces the conversion of some STK38 from its phosphorylated to its non- or hypo-phosphorylated form.

GSK-3 phosphorylation status correlates with STK38 activity

Since CA-AKT1 converted STK38 to its faster-migrating non- or hypo-phosphorylated form (Fig. 2B), we hypothesized that STK38 dephosphorylation was caused by the AKT-mediated inactivation of an STK38 kinase or activation of a protein phosphatase, and set out to identify an STK38-targeting molecule among AKT's substrates. The glycogen synthase kinase 3 (GSK-3) homologues are highly conserved. Two mammalian GSK-3 isoforms have been identified, GSK-3α and GSK-3β, which share 85% amino acid sequence identity and have the same substrate specificity [15]. GSK-3 s are constitutively active but are inhibited by AKT-mediated phosphorylation on S21 of GSK-3α or S9 of GSK-3β [16]. To test whether the GSK-3 phosphorylation status was correlated with STK38 activity, we examined the effect of various stimuli on the phosphorylation levels of GSK-3 s. We used phospho-specific antibodies to detect epitopes on GSK-3 (phospho-S21 of GSK-3α and phospho-S9 of GSK-3β). The phosphorylated GSK-3α/β levels were enhanced 2.5-fold by H_2O_2, but were not enhanced by etoposide, sorbitol, or anisomycin (Fig. 3A).

We further investigated the correlation between GSK-3β phosphorylation status and STK38 activity in one normal and four cancer cell lines. The GSK-3β phosphorylation was analyzed by Western blotting using an anti-phospho (S9) GSK-3β antibody. All five cell lines were found to express both STK38 and GSK-3β. The STK38 activity and GSK-3β phosphorylation were both higher in most of the cancer cell lines than in the normal cell line, Hs27 (Fig. 3B). Of all the cell lines, the STK38 activity and GSK-3β phosphorylation were both lowest in the cancer cell line LU99. In all cases, the STK38 activity was closely correlated with the endogenous GSK-3β phosphorylation level. These results suggest that the phosphorylation or inactivation of GSK-3 s is necessary to stimulate STK38 activity.

Inhibition of GSK-3β results in increased STK38 activity

We next examined the effect of a specific GSK-3β inhibitor, GSK-3β inhibitor VII [17], on the STK38 kinase activity or its SDS-PAGE migration pattern. We first confirmed that the GSK-3β inhibitor

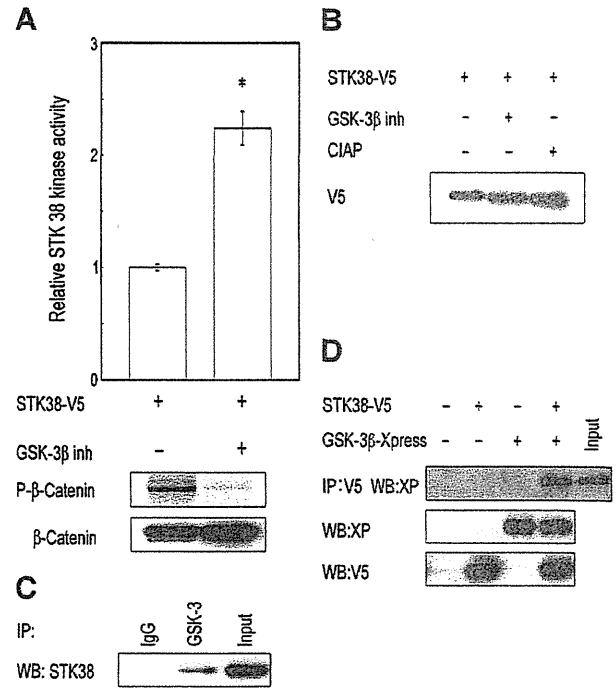

Fig. 4. Inhibition of GSK-3 stimulates STK38 activity and STK38-GSK-3β interaction. (A) Inhibition of GSK-3β stimulates STK38 activity. HEK293T cells were transiently transfected with a mammalian expression vector encoding Wt STK38-V5. Forty-eight hours after transfection, the cells were left untreated or treated with 50 μM GSK-3β inhibitor VII for 30 min. Cell lysates were prepared, and the STK38 kinase activity was measured by immune complex kinase assay with an anti-V5 antibody. Phosphorylation of endogenous β-Catenin was analyzed by Western blotting with a phosphorylated β-Catenin-specific antibody. Data represent the average and standard deviation of three independent experiments. Statistical analysis was performed using the Student's *t*-test. *, $p<0.05$ when compared with the wild type without stimulation was considered significant. (B) HEK293T cells were transfected with V5-tagged STK38, and the cells were left untreated or treated with GSK-3β inhibitor VII as described above. Cell lysates were subjected to Western blotting analysis with the anti-V5 antibody. The cell lysates of the untreated cells were treated with or without CIAP at 30 °C for 20 min before Western blotting analysis. (C) Cell lysates from HeLa cells were subjected to immunoprecipitation (IP) with an anti-rabbit immunoglobulin G or anti-GSK-3β antibody, and the immunoprecipitates were analyzed by Western blotting (WB) with an anti-STK38 antibody. (D) HEK293T cells were transfected with STK38-V5 alone or with Xpress-GSK-3β, and were immunoprecipitated using an anti-V5 antibody. The V5-immunoprecipitates were analyzed by Western blotting with an anti-Xpress antibody (IP: V5, WB: XP). Expression of those tagged-proteins was analyzed by Western blotting with the V5 or Xpress antibody (WB: V5 or XP).

suppressed the phosphorylation of β-Catenin, a substrate for GSK-3, by Western blot using an anti-phospho-β-Catenin antibody. Next, we tested the GSK-3β inhibitor's effect on the activity of V5-tagged STK38, and found that the kinase activity of immunoprecipitated STK38 was enhanced 2.2-fold (Fig. 4A). To confirm that GSK-3 is a negative regulator of STK38, we constructed *gsk-3α* and *gsk-3β* shRNA expression vectors and examined how GSK-3 knockdown affected the STK38 kinase activity. Knockdown of both GSK-3α and GSK-3β stimulated the STK38 activity by 1.9-fold (Supplemental Fig. 2). Moreover, the GSK-3β inhibitor altered the STK38 migration pattern on SDS-PAGE, increasing the amount of the faster-migrating form (Fig. 4B, lane 2). The migration of STK38 treated with a protein phosphatase was also more rapid than the untreated control (Fig. 4B, lane 3), indicating that these faster-migrating bands represented non- or hypo-phosphorylated species. The inhibition of GSK-3 results in the dephosphorylation of its substrates [18]. Thus, our results suggest that the GSK-3 inhibitor prevents GSK-3β from phosphorylating STK38, which results in dephosphorylated, faster-migrating STK38 bands on immunoblots.

STK38 physically interacts with GSK-3β

Given that our results suggested that STK38 is a target of GSK-3, we next investigated whether these two proteins interact physically in intact cells. Endogenous GSK-3β was immunoprecipitated from HeLa cells, and the immunoprecipitates were subjected to Western

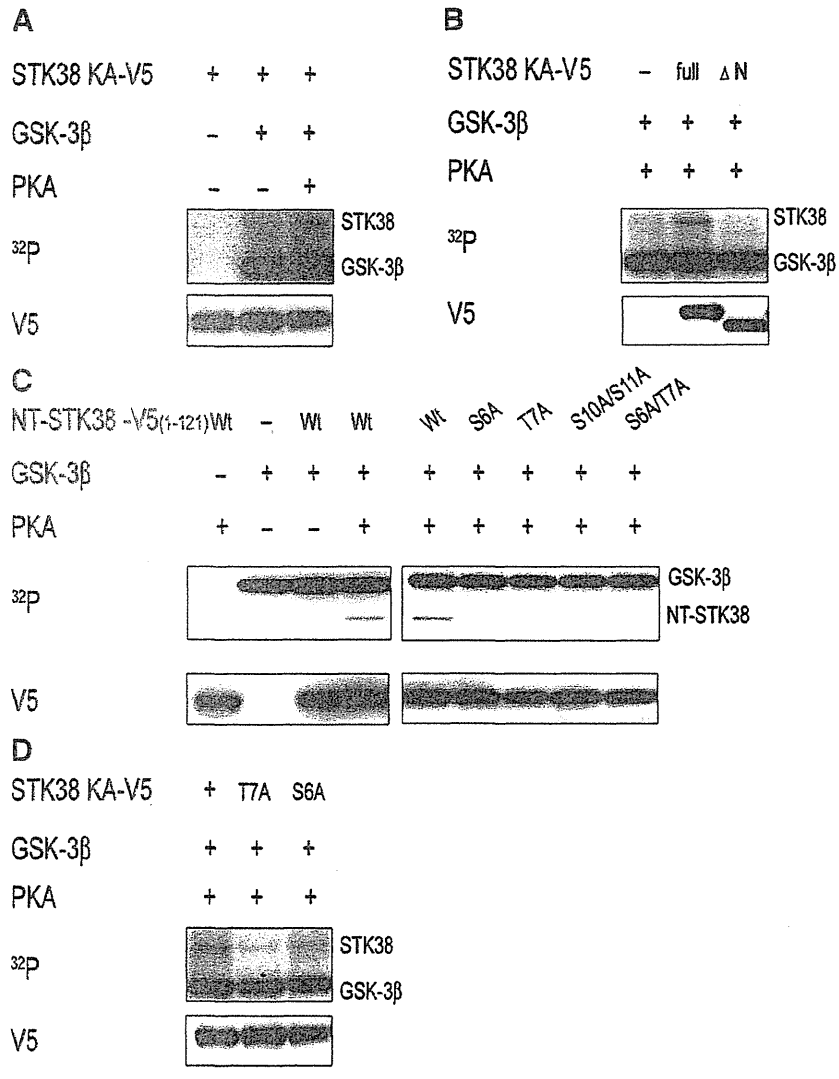

Fig. 5. GSK-3β triggers STK38 phosphorylation on S6 and T7, requiring priming phosphorylation on S10 and S11. (A) GSK-3β efficiently phosphorylates STK38 pretreated with PKA. HEK293T cells were transiently transfected with a mammalian expression vector encoding V5-tagged STK38 K118A (KA). After 48 h, the V5-tagged STK38 was immunopurified using the anti-V5 antibody and subjected to a GSK-3 kinase assay. Briefly, immunopurified STK38 K118A (KA) was left untreated (lane 1), incubated with 100 U of GSK-3β alone in the presence of [γ-^{32}P] ATP (lane 2), or sequentially incubated with 250 U of PKA in the presence of non-radioactive ATP and then 100 U of GSK-3β in the presence of [γ-^{32}P] ATP (lane 3). The kinase reaction products were subjected to SDS-PAGE and analyzed by autoradiography. (B) STK38 is phosphorylated at the N-terminal region by GSK-3β. HEK293T cells were transiently transfected with a mammalian expression vector encoding either V5-tagged full-length or ΔN STK38 K118A (KA) (87–465). After 48 h, each V5-tagged STK38s were immunopurified using the anti-V5 antibody and subjected to the GSK-3 kinase assay as described in panel A. (C) Primed phosphorylation on S10 and S11 allows more efficient GSK-3β-mediated phosphorylation of STK38 on S6 and T7, respectively. Bacterially expressed V5-tagged NT-STK38 (1-121aa) was sequentially incubated with PKA in the presence of non-radioactive ATP and then treated with buffer alone in the presence of [γ-^{32}P] ATP (lane 1). GSK-3β was incubated with buffer alone in the presence of [γ-^{32}P] ATP (lane 2). NT-STK38 was treated with GSK-3β alone in the presence of [γ-^{32}P] ATP (lane 3), or sequentially incubated with PKA in the presence of non-radioactive ATP and then treated with GSK-3β in the presence of [γ-^{32}P] ATP (lanes 4 and 5). V5-tagged NT-STK38 (S6A), -(T7A), -(S10A/S11A), or -(S6A/T7A) was also sequentially incubated with PKA in the presence of non-radioactive ATP and then treated with GSK-3β in the presence of [γ-^{32}P] ATP (lanes 6–9). The kinase reaction products were subjected to SDS-PAGE and then analyzed by autoradiography. (D) Full-length STK38 variants were subjected to the GSK-3 kinase assay as described in panel A. The expression levels of V5-tagged STK38 variants were analyzed by Western blotting with the anti-V5 antibody.

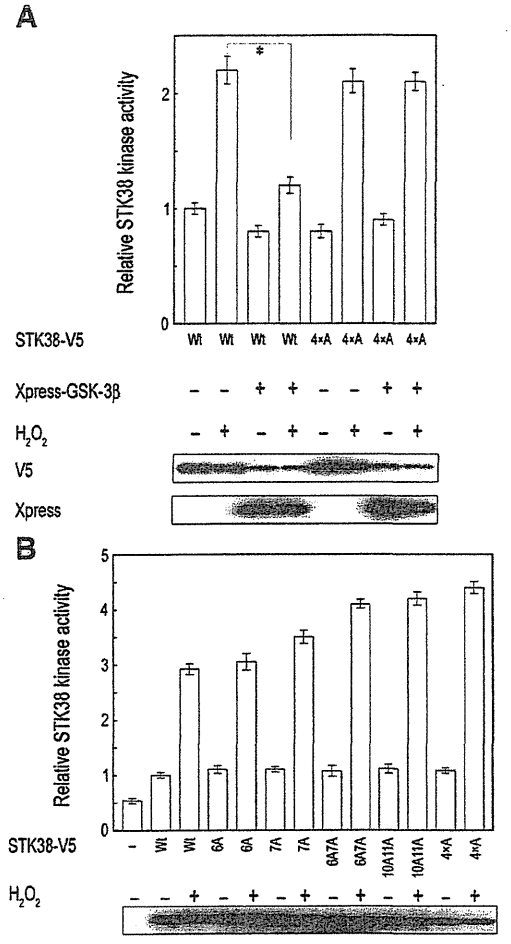

Fig. 6. GSK-3-mediated phosphorylation decreases STK38's kinase activity. (A) Effect of GSK-3β (S9A) overexpression on H_2O_2-stimulated STK38 activity. COS-7 cells were transiently transfected with V5-tagged Wt-STK38 or the 4×A mutant, with or without Xpress-GSK3β (S9A). Forty-eight hours after transfection, the cells were exposed to H_2O_2 (2 mM for 30 min) or left untreated. The V5-tagged STK38s were immediately immunopurified with an anti-V5 antibody, and the individual STK38 kinase activity was measured as described above. The data are representative of five independent experiments. Statistical difference between H_2O_2-treated cells expressing wild type STK38 alone (lane 2) and both wild type STK38 and GSK3β (S9A) (lane 4) is indicated by an astersik (*, $p<0.05$). Expression of the STK38-V5 variants or Xpress-GSK3β (S9A) was analyzed by Western blotting. (B) Both S6 and T7 and/or the priming phosphorylation sites at S10 and S11 of STK38 are required for the negative regulation of STK38. HEK293T cells were transiently transfected with an empty vector or the indicated V5-tagged STK38 phosphorylation mutant. Forty-eight hours after transfection, the cells were left untreated or exposed to H_2O_2 (2 mM for 30 min). The V5-tagged STK38s were immediately immunopurified with the anti-V5 antibody, and the STK38 kinase activity was measured as described above.

blotting with an anti-STK38 antibody. GSK-3β physically interacted with STK38, as shown in Fig. 4C. Next, HEK293T cells were co-transfected with Xpress-tagged GSK-3β and V5-tagged STK38, and were then subjected to co-immunoprecipitation. Western blotting analysis using an anti-Xpress antibody of the V5 immunoprecipitates also revealed that STK38 associated with GSK-3β (Fig. 4D).

STK38 is a GSK-3β target in vitro

To investigate the mechanisms by which GSK-3 regulates STK38, we next examined whether GSK-3 could phosphorylate STK38 directly. GSK-3 is a hierarchical kinase that requires a prior "priming" phosphorylation of its substrate on a serine/threonine (S/T) positioned n +4 from the GSK-3 phosphorylation site (GSK-3 consensus sequences: X (S/T)XXX(S/T-phospho), where X is any amino acid) [19,20]. PKA or CKI can act as a priming kinase for some GSK-3 substrates *in vitro* [21,22]. Therefore, we examined PKA's ability to prime immunopurified full-length STK38 (K118A) for phosphorylation by GSK-3 *in vitro* (Fig. 5A). To control for the possibility that endogenous kinases might co-purify with STK38, we added [γ-^{32}P] ATP alone to the immunopurified kinase-dead mutant STK38 (K118A), and confirmed that no label was incorporated (Fig. 5A, lane1). Non-PKA-treated STK38 (K118A) showed almost no phosphorylation by GSK-3β (Fig. 5A, lane 2). However, when STK38 (K118A) was phosphorylated first with PKA using unlabeled ATP, followed by a separate kinase reaction using GSK-3β with radiolabeled ATP, the label was incorporated into STK38 (K118A); this demonstrated that GSK-3β successfully phosphorylated the STK38 (Fig. 5A, lane 3). We also observed the GSK-3β-mediated phosphorylation of STK38 when STK38 was pre-incubated with CKI (data not shown).

Since STK38 contains multiple potential GSK-3 phosphorylation sites, we produced several STK38 deletion mutants to identify the sites phosphorylated by GSK-3. Deletion of the first 86 residues (1–86) of the N-terminal region significantly blocked the phosphorylation by GSK-3β, even when the deletion mutant (ΔN STK38 KA) was pre-incubated with PKA (Fig. 5B). The N-terminal region of mouse or human STK38 contains two consensus GSK-3 phosphorylation sites. Therefore, we next examined whether GSK-3 could phosphorylate these sites *in vitro*, on a bacterially expressed N-terminal fragment (NT-STK38; residues 1–121). When NT-STK38 was sequentially incubated with PKA in the presence of non-radioactive ATP and then with buffer alone in the presence of [γ-^{32}P] ATP, NT-STK38 was not phosphorylated. This indicated that the latter reaction mixture did not contain residual PKA (Fig. 5C, lane 1). Although NT-STK38 was slightly phosphorylated by GSK-3β alone (Fig. 5C, lane 3), when NT-STK38 was first pretreated with PKA in the presence of non-radioactive ATP and then treated with GSK-3β in the presence of [γ-^{32}P] ATP, GSK-3β effectively phosphorylated it (Fig. 5C, lanes 4 and 5). Replacing S6, T7, or both with alanine completely prevented the phosphorylation by GSK-3β (Fig. 5C, lanes 6, 7, and 9).

To determine whether the phosphorylation of STK38 on residues S10 and S11 primed it for phosphorylation by GSK-3, we assayed the ability of GSK-3β to phosphorylate an NT-STK38 (S10A/S11A) double mutant. We found that GSK-3β phosphorylated the NT-

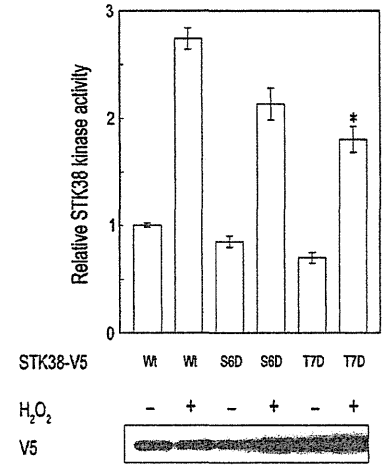

Fig. 7. Phosphomimetic mutation on S6 or T7 of STK38 decreases its kinase activity. HEK293T cells were transiently transfected with the indicated V5-tagged STK38 phosphomimetic mutants. Forty-eight hours after transfection, the cells were exposed to H_2O_2 (2 mM for 30 min) or left untreated. The V5-tagged STK38s were immediately immunopurified with an anti-V5 antibody, and the STK38 kinase activity was measured as described above. Statistical analysis was performed using Student's *t*-test. *, $p<0.05$ when compared with the H_2O_2-treated wild type was considered significant. The expression of individual STK38-V5 variants was analyzed by Western blotting with the anti-V5 antibody.

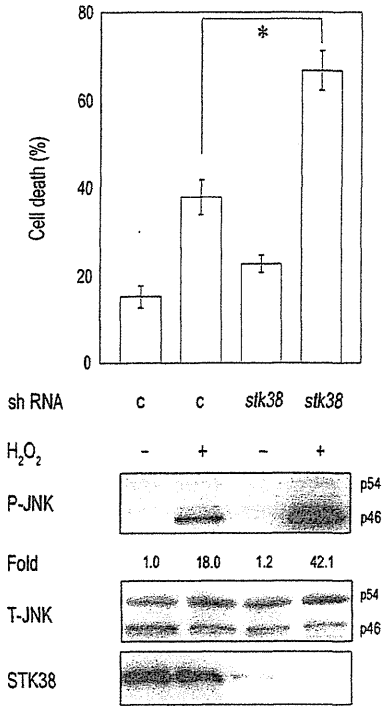

Fig. 8. STK38 inhibits H_2O_2-induced cell death. HeLa cells were transfected with the non-targeting control (c) or *stk38*-specific shRNA expression vector. Twenty-four hours after the transfection, the cells were cultured in medium containing 0.2 μg/ml puromycin for selection, for an additional 48 hours. Then, the transfected cells were either left untreated or treated with 100 μM H_2O_2 for an additional 16 hours. Cell death was assessed by staining with Annexin V-FITC plus PI using a flow cytometer. Statistical difference between H_2O_2–treated cells expressing non-targeting control (lane 2) and *stk38*-specific shRNA (lane 4) is indicated by an astersik (*, $p<0.05$). (upper panel). HeLa cells were transfected with the non-targeting control (c) or *stk38*-specific shRNA expression vector, and selected as described above. The transfected cells were then treated with H_2O_2 (100 μM for 30 min) or left untreated. The cell lysates were subjected to Western blotting analysis with the indicated antibodies (lower panel).

STK38 (S10A/S11) double mutant much less efficiently than NT-STK38 (Fig. 5C, lane 8), even after pretreatment with PKA. The residual phosphorylation of the NT-STK38 (S10A/S11A) double mutant was probably due to priming-independent GSK-3 phosphorylation (Fig. 5C, lane 3). We further assayed whether GSK-3 could phosphorylate immunopurified full-length STK38 on S6 and T7 *in vitro*. The results showed that alanine substitution at S6 or T7 of STK38 (K118A) significantly prevented the phosphorylation by GSK-3β (Fig. 5D). Together, these results indicated that GSK-3β phosphorylates STK38 at S6 and T7 *in vitro*, and does so efficiently when S10 and S11 of STK38 are prephosphorylated by a priming kinase, such as PKA.

S6 and T7 of STK38 are essential for its regulation by GSK-3

To investigate whether GSK-3 regulates STK38 activity, we examined the effects of GSK-3 overexpression on the H_2O_2-stimulated STK38 activity. In COS-7 cells expressing wild-type STK38, the STK38 kinase activity was stimulated 2.2-fold in response to H_2O_2 (Fig. 6A, lane 2). Co-transfection of GSK-3β (S9A) significantly reduced the H_2O_2-stimulated wild-type STK38 kinase activity (Fig. 6A, lane 4), whereas the kinase activity of the STK38 mutant with alanine substitutions at all four residues (S6, T7, S10, and S11), the 4×A mutant, was not affected by GSK-3β (S9A), suggesting that the GSK-3-mediated phosphorylation at S6 and T7 of STK38 is essential for limiting the full STK38 activity (Fig. 6A, lane 8). The co-transfection of GSK-3β (S9A) with STK38 also reduced the expression level of STK38 (Fig. 6A). GSK-3-mediated phosphorylation often triggers the subsequent proteolysis of the substrate [23,24]. However, the STK38 expression level of the quadruple mutant was also decreased by co-expression with GSK-3β (S9A), indicating that the phosphorylation at S6, T7, S10, and S11 of STK38 was not involved in the GSK-3-mediated reduced expression.

To further evaluate the functional significance of the phosphorylation of STK38 by GSK-3, we tested the kinase activities of STK38 mutants with alanine substitutions at GSK-3 phosphorylation sites (S6 and/or T7), the putative priming sites for GSK-3 (S10 and S11), or all four residues (S6, T7, S10, and S11). Mutation at S6 or T7 of STK38 resulted in a respective 3.1- or 3.5-fold enhancement of the STK38 activity in response to H_2O_2, indicating that the phosphorylation at either S6 or T7 modestly reduced the H_2O_2-induced STK38 activation (Fig. 6B, lanes 5 and 7). Substituting alanine at both S6 and T7 of STK38 enhanced the H_2O_2-stimulated STK38 activity 4.1-fold, suggesting that STK38's kinase activity is synergistically attenuated by GSK-3-mediated phosphorylation at S6 and T7 (Fig. 6B, lane 9). Similarly, mutating the priming phosphorylation sites (S10 and S11) increased the H_2O_2-induced STK38 activation 4.2-fold (Fig. 6B, lane 11). The 4×A mutant showed a particularly strong response to H_2O_2 stimulation (Fig. 6B, lane 13). Notably, the STK38 activity in cells expressing the 4×A mutant was almost the same as in those expressing wild-type STK38 without stimulation, indicating that STK38 dephosphorylation at S6, T7, S10, and/or S11 contributes to its full activation.

To confirm the region of STK38 responsible for its regulation, we generated a deletion mutant that lacked the N-terminal region containing both the GSK-3- and priming-phosphorylation sites, named ΔN2 STK38 (residues 12 to 466). We expressed ΔN2 STK38 in HEK293T cells, and assayed its kinase activity. The deletion of the N-terminal 11 residues (1–11) caused a 4.0-fold enhancement of STK38 activity in response to H_2O_2, indicating that these 11 residues comprised the STK38 regulatory region (Supplemental Fig. 3).

Phosphomimetic mutation on S6 or T7 of STK38 reduces its kinase activity

To confirm that the phosphorylation of STK38 on S6 and T7 is essential for the downregulation of its activity, we generated STK38

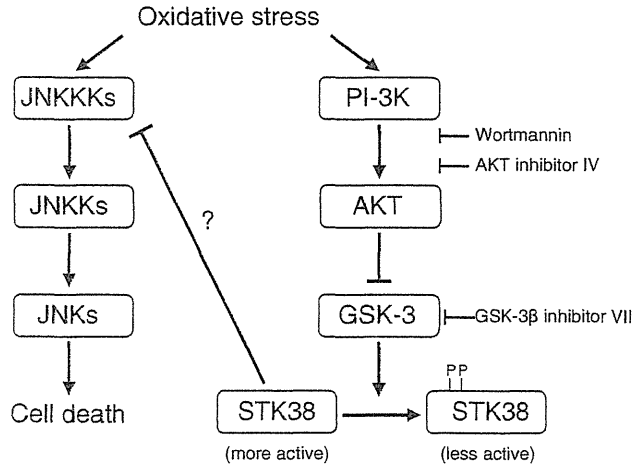

Fig. 9. Model for the oxidative stress-induced activation of the STK38 signaling pathway. Oxidative stress induces the activation of PI-3 K, followed by ATK activation. Although GSK-3 has a high basal activity inside cells and negatively regulates STK38 through its phosphorylation, GSK-3 is inhibited in response to oxidative stress through its AKT-catalyzed phosphorylation. GSK-3 inhibition leads to the dephosphorylation of STK38, resulting in its activation. JNKs are activated through the kinase cascade of JNK kinase (JNKK), and JNKK kinase (JNKKK) by extracellular stresses including oxidative stress. JNKs are often directly linked to cell death. Activated STK38 can interact with some JNKKKs and negatively regulate them (see ref 8), leading to the suppression of oxidative stress-stimulated JNK signal transduction. We used wortmannin as an inhibitor of PI-3 K, AKT inhibitor IV, and GSK-3 inhibitor VII in this study.

mutants with aspartic acid residues at the S6 or T7 position, to mimic phosphorylation. We then tested their response to H_2O_2 in HEK293T cells. The substitution of aspartic acid at T7 caused a reduced basal STK38 kinase activity that was 70% of wild-type STK38, and it significantly reduced the H_2O_2-stimulated STK38 activity to 66% of the activity seen with wild type (Fig. 7). The phosphomimetic mutation at S6 reduced the H_2O_2-stimulated STK38 activity to 78% of that of wild-type STK38. These results indicate that the GSK-3-mediated phosphorylation of STK38 on residues S6 and T7 is essential for the negative regulation of STK38.

Activation of STK38 suppresses H_2O_2-induced JNK phosphorylation and cell death

Activation of the PI-3 K/AKT signaling pathway promotes cell survival and suppresses apoptosis, or cell death [25,26]. We next investigated STK38's possible involvement in regulating cell survival, by examining how it affected H_2O_2-induced cell death. Transfection with *stk38* shRNA, but not with a control expression vector, specifically knocked down the endogenous STK38 expression in HeLa cells. Exposure of HeLa cells expressing the *stk38* shRNA to H_2O_2 resulted in a marked increase in cell death (66.7%), compared to that in cells expressing the control shRNA (37.8%) (Fig. 8, upper panel). Enhanced cell death was also observed in the STK38 knockdowned cells after transient exposure to high concentration H_2O_2 (Supplemental Fig. 4). However, the apoptosis rate was not significantly higher in the STK38 knockdowned cells than that of the control after treatment with 100 μM or 2 mM H_2O_2 (data not shown).

Oxidative stress causes cells to activate the JNK pathway, which is one of three major MAPK-signaling pathways [13,27]. In several cell types, JNKs are directly linked to cell death, including apoptosis and necrosis [28,29]. We previously demonstrated that STK38 inhibits the JNK kinase kinases MEKK1/2 [8]. Therefore, we examined how the knockdown of STK38 affected the H_2O_2-induced activation of JNK signaling. Although the *stk38*-specific shRNA did not affect the expression level of total JNKs, the knockdown of STK38 enhanced the H_2O_2-induced phosphorylation of JNK, compared with the effect of the non-targeting control shRNA (Fig. 8, lower panel). These results indicate that STK38 inhibits H_2O_2-induced cell death by attenuating the stress-activated JNK signaling.

Discussion

In this paper, we identified GSK-3 as a STK38 kinase and demonstrated that H_2O_2-stimulated STK38 kinase activity is downregulated by its GSK-3-mediated phosphorylation on S6 and T7. We have provided several lines of evidence that GSK-3 regulates STK38. First, STK38 was significantly stimulated by H_2O_2 (Fig. 1A, B, and supplemental Fig. 1A), and its H_2O_2-induced activation was inhibited by the PI-3 K inhibitor wortmannin or by AKT inhibitor IV (Figs. 1C and 2A). STK38 was also activated by the overexpression of a constitutively active form of AKT-1 (CA-AKT1) (Fig. 2B). We found that H_2O_2 stimulation enhanced the phosphorylation of AKT (active form of AKT) and GSK-3 (inactive form of GSK-3) (Figs. 1D and 3A). Our study's results are consistent with previous reports that GSK-3 has high basal activity within the cell, but is inhibited in response to extracellular signals through the AKT/protein kinase B (PKB)-catalyzed phosphorylation of an N-terminal serine residue (S21 of GSK-3α; S9 of GSK-3β) [16,18,26]. GSK-3 inhibition leads to the dephosphorylation—and often, activation—of its substrate [30]. We demonstrated that the STK38 activity was stimulated by GSK-3β inhibitor VII (Fig. 4A), and that STK38's non- or hypo-phosphorylated forms increased quite noticeably when HEK293T cells were either co-transfected with CA-AKT1 or treated with a GSK-3β inhibitor (Figs. 2D and 4B). Our results also showed a correlation between the GSK-3 phosphorylation level and STK38 activity (Fig. 3). Together, our findings suggest that AKT facilitates STK38 dephosphorylation by inhibiting GSK-3 and stimulates STK38 activity. After H_2O_2 treatment, the faster-migrating non-phosphorylated form of STK38 was not observed. STK38 may be subjected to multiple post-translational modifications in response to H_2O_2.

Second, we demonstrated that GSK-3β interacted with STK38 (Fig. 4C and D), that GSK-3β phosphorylated residues S6 and T7 of STK38 (and did so efficiently following PKA pretreatment),.and that mutations at two priming phosphorylation sites (S10/S11) attenuated the phosphorylation of two other sites S6/T7 by GSK-3 *in vitro* (Fig. 5). These results indicate that phosphorylation at S10 or S11 is the respective priming event for GSK-3-mediated STK38 phosphorylation on S6 or T7. We also tested whether other putative GSK-3-phosphorylation sites were phosphorylated *in vitro*. However, replacing at least T185, T326, or S403 with alanine had no effect on the phosphorylation of STK38 by GSK-3β (data not shown).

GSK-3 phosphorylates and regulates a number of important cellular targets involved in various pathologies, such as diabetes, Alzheimer's disease, and cancer [19,31-33], and in apoptosis [34]. Phosphorylation by GSK-3 often inhibits its substrates [30,31]. Our findings showed that overexpression of GSK-3β (S9A) inhibited the H_2O_2-stimulated activation of STK38, whereas the H_2O_2-stiumulated STK38 activity of the 4×A mutant (S6A/T7A/S10A/S11A) was not affected by GSK-3β (Fig. 6A), suggesting the involvement of specific phosphorylation events in GSK-3-mediated inhibition. Replacing both GSK-3 phosphorylation sites on STK38 with alanine (S6A/T7A) enhanced the H_2O_2-induced STK38 activity (Fig. 6B). We did not detect a significant difference in kinase activity between the STK38 S6A/T7A mutant and the one whose priming phosphorylation sites were mutated (S10A/S11A), suggesting that the main role of the phosphorylated residues S10 and S11 is to prime STK38 for its efficient phosphorylation by GSK-3. On the other hand, the substitution of alanine at the GSK-3 phosphorylation and/or the priming sites did not affect the basal STK38 activity, suggesting that dephosphorylation of these sites of STK38 may be a priming event for its full activation. Moreover, phosphomimetic mutation of S6 or T7 partially decreased the H_2O_2-stimulated STK38 activity (Fig. 7). These results suggest that the GSK-3-mediated phosphorylation of both S6 and T7 of STK38 synergistically limits its full activity.

In contrast, some evidence suggests that the N-terminal region of STK38 contains functional domains responsible for its positive regulation. Ca^{2+}/S100B interacts with the N-terminal regulatory (NTR) domain (residues 1–87) of STK38 and stimulates its activity [35]. STK38 has a unique basic-residue-rich insert (residues 244–276) in the catalytic domain, and is autoinhibited by it. Mob (Mps one binder) associates with the NTR domain of STK38, and this interaction releases the auto-inhibition, permitting the efficient autophosphorylation of STK38 on S281, which is in the activation segment, and thus activates STK38 activity [36,37]. Although S281 of STK38 is a putative GSK-3 phosphorylation site, this residue is conserved among STK38 and its relatives and is essential for their full activation [38]. These findings indicate that the N-terminal region of STK38 is required for modulator binding to STK38. In contrast, our study focuses on the phosphorylation of residues within STK38's NTR domain, and provides the first demonstration that phosphorylation on S6 and T7 or S10 and S11 is required to limit full STK38 activity. Together, phosphorylation of STK38 on S6, T7, S10, and S11 may alter the binding affinity of its modulators such as Mob for the NTR domain and/or affect the autophosphorylation of STK38 on S281 in the activation segment.

Previous reports have suggested that STK38 might function as a proto-oncogene. STK38 is up-regulated in progressive ductal carcinoma *in situ*, and in some melanoma cell lines [35,39]. Here we also found that the STK38 activity was slightly elevated in most cancer cell lines tested (Fig. 3B). In this regard, STK38 dysregulation may